

Nonadiabatic Field with Triangle Window Functions on Quantum Phase Space

*Xin He, Xiangsong Cheng, Baihua Wu, and Jian Liu**

Beijing National Laboratory for Molecular Sciences, Institute of Theoretical and Computational
Chemistry, College of Chemistry and Molecular Engineering,

Peking University, Beijing 100871, China

(Submitted on March 14, 2024)

AUTHOR INFORMATION

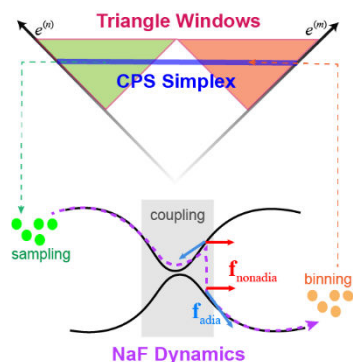
Corresponding Author

* Electronic mail: jianliupku@pku.edu.cn

Abstract

The *constraint coordinate-momentum phase space* (CPS) formulation of finite-state quantum systems has recently revealed that the triangle window function approach is an isomorphic representation of the exact population-population correlation function of the two-state system. We use the triangle window (TW) function and the CPS mapping kernel element to formulate a novel useful representation of discrete electronic degrees of freedom (DOFs). When it is employed with nonadiabatic field (NaF) dynamics, a new variant of the NaF approach (i.e., NaF-TW) is proposed. Extensive benchmark tests of model systems in both the condensed phase and gas phase demonstrate that the NaF-TW approach is competent in faithfully capturing the dynamical interplay between electronic and nuclear DOFs. In comparison to the symmetrical quasi-classical (SQC) method where triangle window functions were originally proposed, the performance of NaF-TW is significantly better when the bifurcation characteristic of nuclear motion in the asymptotic region is important.

TOC GRAPHICS



KEYWORDS. Nonadiabatic dynamics, constraint phase space, nonadiabatic field, triangle windows

Nonadiabatic transition dynamics is crucial in understanding many important light-driven, photo-emission, charge transfer, and cavity modified phenomena in natural and artificial complex molecular systems in chemistry, materials, biology, quantum information and computation, environmental science, and so forth¹⁻¹⁴. In these systems, we often depict electrons by *discrete* electronic states and nuclei in continuous coordinate space. Numerical simulations of such composite systems often employ two prevailing categories of practical dynamics approaches with independent trajectories. The first category uses Born-Oppenheimer (BO) trajectories generated from different single potential energy surfaces (PESs). The surface hopping approach pioneered by Tully and coworkers¹⁵⁻¹⁷ has been modified by various hopping algorithms¹⁸⁻²⁹ for connecting two independent Born-Oppenheimer trajectories on two different adiabatic PESs. The category of BO-trajectory-based dynamics often meets the challenge for nonadiabatic processes where the states remain coupled all the time, especially when the temperature is relatively low. Another category utilizes the mean field trajectory in the spirit of the Ehrenfest theorem³⁰. In addition to the original Ehrenfest dynamics³⁰ for nonadiabatic transitions³¹⁻³³, a few Ehrenfest-like dynamics approaches³⁴⁻⁵⁴ have been developed since the Meyer-Miller mapping Hamiltonian model was proposed for treating both nuclear and electronic DOFs on the same footing^{34, 55}. Among these Ehrenfest-like dynamics approaches, the symmetrical quasi-classical (SQC) method for nonadiabatic dynamics^{45-47, 49, 50} is of particular interest. In the latest version of the SQC method, Cotton and Miller introduced the triangle window function (TWF) approach for discrete electronic DOFs^{46, 49, 50}. The TWF approach was empirically proposed but reasonably accurate for electronic dynamics (in the frozen-nuclei limit) even in the weak state-state coupling region⁴⁶. In addition that the TWF approach offers the initial condition as well as the integral expression of the time-dependent physical property for electronic DOFs, the independent quasi-classical trajectory is

generated from Ehrenfest-like dynamics of the Meyer-Miller mapping Hamiltonian³⁴. The SQC with TWF for nonadiabatic dynamics^{46, 47, 49} has widely been applied to various condensed-phase system-bath models as well as realistic molecular systems^{50, 56-65}. The category of mean field trajectory-based dynamics methods performs well in the nonadiabatic state-state coupling region, but is more difficult in capturing the bifurcation characteristic of the nuclear motion in the asymptotic region where the state-state coupling disappears. In addition to the two major categories, there are some other methods using independent trajectories⁶⁶⁻⁶⁸.

The unified phase space formulation with coordinate-momentum variables offers an exact interpretation of quantum mechanics to describe composite systems⁶⁹⁻⁷⁶, where the *constraint* coordinate-momentum *phase space* (CPS) representation is used for *discrete* (electronic) degrees of freedom (DOFs) while the infinite (Wigner) coordinate-momentum phase space representation is used for *continuous* (nuclear) DOFs. The CPS representation (of discrete electronic DOFs) related to the quotient space $U(F)/U(F-1)$ was first introduced to nonadiabatic dynamics by the sphere representation with coordinate-momentum variables in Section II of Ref⁷¹ and by the simplex representation with action-angle variables in Appendix A of Ref⁷¹. It was shortly developed to a generalized phase space formulation, CPS with commutator variables^{73, 74} in spirit of refs⁶⁹⁻⁷¹, which is related to the quotient space $U(F)/U(F-r)$ (with $1 \leq r < F$), namely the complex Stiefel manifold⁷⁷⁻⁷⁹. The exact equations of motion (EOMs) of mapping coordinate-momentum variables of CPS for the pure finite-state quantum system are linear⁷⁵, which is superior to the conventional phase space approaches with angle variables⁸⁰⁻⁸³ used in physics for studying dynamics of composite systems. The unified phase space formulation has recently led to a conceptually novel trajectory-based approach in the adiabatic representation of electronic states, nonadiabatic field (NaF) that is promising in faithfully describing both nuclear motion and

electronic coherence/dissipation⁸⁴. In the state-state coupling region, the nuclear EOMs of the independent trajectory of NaF involve an important nonadiabatic nuclear force term in addition to an adiabatic nuclear force term of a single electronic state (either stochastically with electronic weights or deterministically with the dominant electronic weight). This is substantially different from the two conventional categories of nonadiabatic dynamics methods that involve either BO trajectories on different PESs or mean field trajectories.

The NaF strategy⁸⁴ has been applied to the framework of Ehrenfest dynamics³⁰, fewest-switches surface hopping (FSSH)^{15, 16}, and CPS with commutator variables^{71, 73-75, 85}. The investigation suggests that the nuclear EOMs of the NaF strategy should considerably improve over various surface hopping and Ehrenfest-like dynamics methods. It also indicates that the key of the most successful NaF approach includes the exact phase space representation of discrete electronic DOFs⁸⁴, which offers a consistent way in dealing with the other two critical properties of a trajectory-based quantum dynamics method⁷⁵, namely, the initial condition of the trajectory and the integral expression for evaluation of the time-dependent physical property.

In the letter, we employ the triangular window function⁴⁶, in addition to the original mapping kernel of the $U(F)/U(F-1)$ CPS^{71, 72}, to formulate a novel representation of discrete (electronic) DOFs, which is applied with the NaF strategy to offer a more consistent trajectory-based approach for studying nonadiabatic transition dynamics.

Assume a coupled F -electronic-state Hamiltonian operator of the composite system

$$\hat{H} = \sum_{n,m=1}^F H_{nm}(\mathbf{R}, \mathbf{P}) |n\rangle \langle m|, \quad (1)$$

where $\{\mathbf{R}, \mathbf{P}\}$ are the coordinate and momentum variables for the nuclear DOFs, and $\{|n\rangle\}, n \in \{1, \dots, F\}$ is the “complete” set of orthonormal electronic states (F is in general infinite

when the set of electronic states is rigorously complete). Consider the composite system in the frozen-nuclei limit of eq (1), where each element $H_{nm}(\mathbf{R}, \mathbf{P}) \equiv H_{nm}$ is constant and the Hamiltonian operator of eq (1) becomes $\hat{H} = \sum_{n,m=1}^F H_{nm} |n\rangle\langle m|$, which is the pure F -state quantum system. A generalization of the idea of the exact weighted CPS representation of ref ⁷⁵ implies that the integrand function on electronic mapping CPS is not limited to the product of the element of the mapping kernel and that of the inverse mapping kernel of electronic DOFs⁸⁶. The general phase space expression of the time correlation function between $|n\rangle\langle m|$ and $|k\rangle\langle l|$ reads

$$\begin{aligned} & \text{Tr}_e \left[|n\rangle\langle m| e^{i\hat{H}t} |k\rangle\langle l| e^{-i\hat{H}t} \right] \\ &= \left(C_{nm,kl}(t) \right)^{-1} \int d\boldsymbol{\gamma} w(\boldsymbol{\gamma}) \int_{\mathcal{S}(\mathbf{x}, \mathbf{p}, \boldsymbol{\Gamma}; \boldsymbol{\gamma})} F d\mathbf{x} d\mathbf{p} d\boldsymbol{\Gamma} \mathbf{G}_{nm,kl}(\mathbf{x}, \mathbf{p}, \boldsymbol{\Gamma}; \boldsymbol{\gamma}; t) \end{aligned} \quad (2)$$

where $\text{Tr}_e[]$ represents the trace over electronic DOFs, $\{\mathbf{x}, \mathbf{p}\} = \{x^{(1)}, \dots, x^{(F)}, p^{(1)}, \dots, p^{(F)}\}$ are the mapping coordinate and momentum variables for discrete electronic DOFs, $\boldsymbol{\Gamma}$ is the $F \times F$ commutator matrix^{69, 73} that can be expressed by auxiliary coordinate-momentum variables,

$$\boldsymbol{\Gamma}_{mn} = \sum_{k=1}^F s_k \left(\xi_k^{(m)} + i\pi_k^{(m)} \right) \left(\xi_k^{(n)} - i\pi_k^{(n)} \right) / 2. \quad (3)$$

In eq (2), $F d\mathbf{x} d\mathbf{p} d\boldsymbol{\Gamma}$ with $d\boldsymbol{\Gamma} = \prod_{k,m=1}^F d\xi_k^{(m)} d\pi_k^{(m)}$ is the integral measure, $\mathcal{S}(\mathbf{x}, \mathbf{p}, \boldsymbol{\Gamma}; \boldsymbol{\gamma})$ defines the phase space constraint that involves parameters $\boldsymbol{\gamma}$, $w(\boldsymbol{\gamma})$ is the quasi-distribution of parameter vector $\boldsymbol{\gamma}$, and $C_{nm,kl}(t)$ is the time-dependent normalization factor. $\mathbf{G}_{nm,kl}(\mathbf{x}, \mathbf{p}, \boldsymbol{\Gamma}; \boldsymbol{\gamma}; t)$ defines the integrand function on the phase space corresponding to $|n\rangle\langle m|$ at time 0 and $e^{i\hat{H}t} |k\rangle\langle l| e^{-i\hat{H}t}$ at time t , which is a generalization of $K_{mn}(\mathbf{x}, \mathbf{p}, \boldsymbol{\Gamma}) K_{lk}^{-1}(\mathbf{x}, \mathbf{p}, \boldsymbol{\Gamma}; t)$, the product of the element of the

mapping kernel and that of its inverse mapping kernel of our CPS formulations^{69-76, 79, 87}. (The convention $\hbar = 1$ is used for discrete electronic DOFs throughout the paper.)

The general expression of the time correlation function eq (2) with trajectory-based dynamics becomes

$$\text{Tr}_e \left[|n\rangle\langle m| e^{i\hat{H}t} |k\rangle\langle l| e^{-i\hat{H}t} \right] \mapsto \left(\bar{C}_{nm,kl}(t) \right)^{-1} \int w(\gamma) d\gamma \int_{S(\mathbf{x}_0, \mathbf{p}_0, \Gamma_0; \gamma)} F d\mathbf{x}_0 d\mathbf{p}_0 d\Gamma_0 \bar{G}_{nm,kl} \left(\{ \mathbf{x}, \mathbf{p}, \Gamma \}_{0 \leq \tau \leq t}; \gamma; t \right), \quad (4)$$

where $\{ \mathbf{x}, \mathbf{p}, \Gamma \}_{0 \leq \tau \leq t}$ denotes the trajectory on the phase space, $\bar{G}_{nm,kl} \left(\{ \mathbf{x}, \mathbf{p}, \Gamma \}_{0 \leq \tau \leq t}; \gamma; t \right)$ defines the integrand function on the phase space corresponding to $|n\rangle\langle m|$ at time 0 and $e^{i\hat{H}t} |k\rangle\langle l| e^{-i\hat{H}t}$ at time t for trajectory dynamics, and $\bar{C}_{nm,kl}(t)$ is the time-dependent normalization factor of the trajectory-based dynamics approach. The expression of eq (4) is a generalization of the formalisms in the CPS formulation^{69-76, 79, 87}, where the trajectory is generated by the linear EOMs yielded from the symplectic structure of CPS.

Our work of ref⁸⁶ presents a new class of isomorphic representations of the exact population-population correlation function of the pure two-state quantum system (i.e., $F = 2$). Remarkably, the TWF approach (for discrete electronic DOFs) proposed by Cotton and Miller⁴⁶, which is practically useful but generally believed to be *ad hoc*, is proved as a special case of the new class of phase space representations for *exact* population dynamics⁸⁶. The proof involves the projection of the TWF onto the $U(F)/U(F-1)$ CPS for the two-state system and integral identities for the exact population-population correlation function. Because the TWF approach is exact for population dynamics of the two-state system⁸⁶ and reasonably accurate for that of the multi-state system (i.e., $F \geq 3$)⁴⁶, it suggests that the triangle window function should be valuable for

developing a novel useful representation of discrete electronic DOFs (e.g., for nonadiabatic dynamics).

Consider the pure F -state system of eq (1). We focus on a special class of eq (4),

$$\begin{aligned} & \text{Tr}_e \left[|n\rangle \langle m| e^{i\hat{H}t} |k\rangle \langle l| e^{-i\hat{H}t} \right] \\ & \mapsto \left(\bar{C}_{nm,kl}(t) \right)^{-1} \int d\boldsymbol{\gamma} w(\boldsymbol{\gamma}) \int_{\mathcal{S}(\mathbf{x}_0, \mathbf{p}_0, \boldsymbol{\Gamma}_0; \boldsymbol{\gamma})} F d\mathbf{x}_0 d\mathbf{p}_0 d\boldsymbol{\Gamma}_0 \bar{\mathbf{G}}_{nm,kl}(\mathbf{x}_0, \mathbf{p}_0, \boldsymbol{\Gamma}_0; \mathbf{x}_t, \mathbf{p}_t, \boldsymbol{\Gamma}_t) \end{aligned} \quad (5)$$

Equation (5) includes four kinds of time correlation functions of electronic DOFs, namely, population-population ($n = m$ and $k = l$), population-coherence ($n = m$ and $k \neq l$), coherence-population ($n \neq m$ and $k = l$), and coherence-coherence ($n \neq m$ and $k \neq l$) correlation functions. Commutator matrix $\boldsymbol{\Gamma}$ can be constant, $\boldsymbol{\Gamma} = \gamma \mathbf{1}$, where γ is a scalar parameter and $\mathbf{1}$ is the identity matrix. In this case, the constraint of CPS reads

$$\mathcal{S}(\mathbf{x}, \mathbf{p}; \gamma) = \delta \left(\sum_{n=1}^F \frac{1}{2} \left((x^{(n)})^2 + (p^{(n)})^2 \right) - (1 + F\gamma) \right) \quad (6)$$

with parameter $\gamma \in (-1/F, \infty)$, and

$$\int_{\mathcal{S}(\mathbf{x}, \mathbf{p}; \gamma)} F d\mathbf{x} d\mathbf{p} g(\mathbf{x}, \mathbf{p}) = \int F d\mathbf{x} d\mathbf{p} \frac{1}{\Omega(\gamma)} \mathcal{S}(\mathbf{x}, \mathbf{p}; \gamma) g(\mathbf{x}, \mathbf{p}) \quad (7)$$

where $\Omega(\gamma)$ is the normalization factor^{71, 72, 75}

$$\Omega(\gamma) = \int d\mathbf{x} d\mathbf{p} \mathcal{S}(\mathbf{x}, \mathbf{p}; \gamma) = \frac{(2\pi)^F (1 + F\gamma)^{F-1}}{(F-1)!} \quad (8)$$

By employing a generalization of the weighted constraint phase space⁷⁵, the expressions of time correlation functions read

$$\begin{aligned} & \text{Tr}_e \left[|n\rangle \langle m| e^{i\hat{H}t} |k\rangle \langle l| e^{-i\hat{H}t} \right] \\ & \mapsto \left(\bar{C}_{nm,kl}(t) \right)^{-1} \int_{-1/F}^{+\infty} w(\gamma) d\gamma \int_{\mathcal{S}(\mathbf{x}_0, \mathbf{p}_0; \gamma)} F d\mathbf{x}_0 d\mathbf{p}_0 \bar{\mathbf{G}}_{nm,kl}(\mathbf{x}_0, \mathbf{p}_0; \mathbf{x}_t, \mathbf{p}_t) \end{aligned} \quad (9)$$

For example, the CMM approach of ref⁶⁹ can be re-interpreted by eq (9) with $w(\gamma) = \delta(\gamma - \gamma_0)$ and $\bar{\mathbf{G}}_{nm,kl}(\mathbf{x}_0, \mathbf{p}_0; \mathbf{x}_t, \mathbf{p}_t) = K_{mn}(\mathbf{x}_0, \mathbf{p}_0) K_{lk}^{-1}(\mathbf{x}_t, \mathbf{p}_t)$, where $K_{mn}(\mathbf{x}, \mathbf{p})$ and $K_{lk}^{-1}(\mathbf{x}_t, \mathbf{p}_t)$ are matrix elements of eqs (7)-(8) of ref⁶⁹ with phase space parameter γ_0 , respectively. In this letter, we employ the TWF⁴⁶ for the electronic correlation function. The expressions read

$$\begin{aligned} & \text{Tr}_e \left[|n\rangle \langle m| e^{i\hat{H}t} |k\rangle \langle l| e^{-i\hat{H}t} \right] \\ & \mapsto \left(\bar{C}_{nm,kl}(t) \right)^{-1} \int_0^{1-1/F} w(\gamma) d\gamma \int_{S(\mathbf{x}_0, \mathbf{p}_0; \gamma)} F d\mathbf{x}_0 d\mathbf{p}_0 \bar{\mathbf{G}}_{nm,kl}(\mathbf{x}_0, \mathbf{p}_0; \mathbf{x}_t, \mathbf{p}_t), \\ & = \left(\bar{C}_{nm,kl}(t) \right)^{-1} \int d\mathbf{x}_0 d\mathbf{p}_0 \frac{F \cdot F!}{(2\pi)^F (F^F - 1)} \bar{\mathbf{G}}_{nm,kl}(\mathbf{x}_0, \mathbf{p}_0; \mathbf{x}_t, \mathbf{p}_t) \end{aligned} \quad (10)$$

where $w(\gamma) = \frac{F^2}{F^F - 1} (1 + F\gamma)^{F-1}$ and $\int_0^{1-1/F} w(\gamma) d\gamma = 1$. In the expression of

$\text{Tr}_e \left[|n\rangle \langle n| e^{i\hat{H}t} |m\rangle \langle m| e^{-i\hat{H}t} \right]$ of eq (10),

$$\bar{\mathbf{G}}_{nn,mm}(\mathbf{x}_0, \mathbf{p}_0; \mathbf{x}_t, \mathbf{p}_t) = \bar{w}_n^{\text{SQC}}(\mathbf{x}_0, \mathbf{p}_0) K_{nn}^{\text{SQC}}(\mathbf{x}_0, \mathbf{p}_0) K_{mm}^{\text{bin}}(\mathbf{x}_t, \mathbf{p}_t), \quad (11)$$

where

$$\bar{w}_n^{\text{SQC}}(\mathbf{x}_0, \mathbf{p}_0) = \frac{2(F^F - 1)}{F \cdot F!} \left(2 - \frac{1}{2} \left((x_0^{(n)})^2 + (p_0^{(n)})^2 \right) \right)^{2-F}. \quad (12)$$

The time-dependent normalization factor reads

$$\begin{aligned} \bar{C}_{nn,mm}(t) &= \sum_{k=1}^F \int_0^{1-1/F} w(\gamma) d\gamma \int_{S(\mathbf{x}_0, \mathbf{p}_0; \gamma)} F d\mathbf{x}_0 d\mathbf{p}_0 \bar{\mathbf{G}}_{nm,kk}(\mathbf{x}_0, \mathbf{p}_0; \mathbf{x}_t, \mathbf{p}_t) \\ &= \sum_{k=1}^F \int d\mathbf{x}_0 d\mathbf{p}_0 \frac{F \cdot F!}{(2\pi)^F (F^F - 1)} \bar{\mathbf{G}}_{nm,kk}(\mathbf{x}_0, \mathbf{p}_0; \mathbf{x}_t, \mathbf{p}_t) \end{aligned}, \quad (13)$$

whose initial value $\bar{C}_{nn,mm}(0)$ is 1.

The TWF for $|n\rangle \langle n|$, the population of n -th state at time 0, is an indicator function,

$$K_{nm}^{\text{SQC}}(\mathbf{x}_0, \mathbf{p}_0) \equiv \begin{cases} 1 & \text{if } (\mathbf{x}_0, \mathbf{p}_0) \in \mathcal{M}_n \\ 0 & \text{otherwise} \end{cases}, \quad (14)$$

where \mathcal{M}_n includes the following set of phase space points,

$$\mathcal{M}_n(\mathbf{x}, \mathbf{p}) : \left\{ (\mathbf{x}, \mathbf{p}) \left| \begin{array}{l} 1 \leq \frac{1}{2} \left((x^{(n)})^2 + (p^{(n)})^2 \right) \leq 2; \\ \forall k \neq n, \frac{1}{2} \left((x^{(k)})^2 + (p^{(k)})^2 + (x^{(n)})^2 + (p^{(n)})^2 \right) \leq 2 \end{array} \right. \right\}. \quad (15)$$

For any point (\mathbf{x}, \mathbf{p}) in $\mathcal{M}_n(\mathbf{x}, \mathbf{p})$, the value of $\sum_{n=1}^F \frac{1}{2} \left((x^{(n)})^2 + (p^{(n)})^2 \right)$ lies in region $[1, F]$, so that

the domain of γ is $\gamma \in [0, 1 - 1/F]$.

The TWF for $e^{i\hat{H}t} |m\rangle \langle m| e^{-i\hat{H}t}$, the population of m -th state at time t , is also an indicator function,

$$K_{mm}^{\text{bin}}(\mathbf{x}_t, \mathbf{p}_t) \equiv \begin{cases} 1 & \text{if } (\mathbf{x}_t, \mathbf{p}_t) \in \mathcal{M}_m^{\text{bin}} \\ 0 & \text{otherwise} \end{cases}, \quad (16)$$

where

$$\mathcal{M}_m^{\text{bin}}(\mathbf{x}, \mathbf{p}) : \left\{ (\mathbf{x}, \mathbf{p}) \left| \begin{array}{l} 1 \leq \frac{1}{2} \left((x^{(m)})^2 + (p^{(m)})^2 \right); \\ \forall k \neq m, \frac{1}{2} \left((x^{(k)})^2 + (p^{(k)})^2 \right) \leq 1 \end{array} \right. \right\}. \quad (17)$$

Because functions $K_{nm}^{\text{SQC}}(\mathbf{x}_0, \mathbf{p}_0)$ and $K_{mm}^{\text{bin}}(\mathbf{x}_t, \mathbf{p}_t)$ of eq (10) and eq (13) are always non-negative, the population-population correlation function remains positive-definite all the time for the choice of the electronic basis set $\{|n\rangle\}$ of eq (1). The expression of eq (10) for the population-population correlation function is exact for only the pure two-state system. We note that the phase space formalism of eqs (10)-(11) is not the only option, and an alternative formulation derived for triangle window functions is presented in Section S5 of the Supporting Information.

Unfortunately, the SQC approach with either triangle or square window functions^{46, 88} does not lead to exact results for the other three kinds of electronic correlation functions even for the pure two-state case ($F = 2$). It is crucial to construct the new phase space representation with the triangle window function used in eqs (14)-(15) for the initial condition such that the other three kinds of electronic correlation functions are exact. Here, we employ the element of the mapping kernel of the $U(F) / U(F - 1)$ CPS^{71, 72} to accomplish the task.

In the expression of eq (10) for $\text{Tr}_e \left[|n\rangle\langle n| e^{i\hat{H}t} |k\rangle\langle l| e^{-i\hat{H}t} \right]$ with $k \neq l$, the population-coherence correlation function,

$$\bar{G}_{nm,kl}(\mathbf{x}_0, \mathbf{p}_0; \mathbf{x}_t, \mathbf{p}_t) = \bar{w}_n^{\text{SQC}}(\mathbf{x}_0, \mathbf{p}_0) K_{nm}^{\text{SQC}}(\mathbf{x}_0, \mathbf{p}_0) K_{lk}^{\text{CMM}}(\mathbf{x}_t, \mathbf{p}_t), \quad (18)$$

where

$$K_{lk}^{\text{CMM}}(\mathbf{x}_t, \mathbf{p}_t) \equiv \frac{1}{2} (x_t^{(l)} + ip_t^{(l)}) (x_t^{(k)} - ip_t^{(k)}) \quad (19)$$

is the element of the mapping kernel of the $U(F) / U(F - 1)$ CPS^{71, 72}. The time-dependent normalization factor of eq (5) is constant, $\bar{C}_{nm,kl}(t) \equiv 1$.

When the initial electronic density matrix includes the coherence term, $|n\rangle\langle m|$ (where $n \neq m$), in the expression of eq (10) for both the coherence-population (where $n \neq m$ and $k = l$) and coherence-coherence (where $n \neq m$ and $k \neq l$) correlation functions,

$$\bar{G}_{nm,kl}(\mathbf{x}_0, \mathbf{p}_0; \mathbf{x}_t, \mathbf{p}_t) = \bar{w}_{nm}^{\text{coh}}(\mathbf{x}_0, \mathbf{p}_0) K_{nm}^{\text{CMM}}(\mathbf{x}_0, \mathbf{p}_0) K_{lk}^{\text{CMM}}(\mathbf{x}_t, \mathbf{p}_t), \quad (20)$$

where $\bar{w}_{nm}^{\text{coh}}(\mathbf{x}_0, \mathbf{p}_0) = \frac{6}{5} \sum_{i=n,m} \bar{w}_i^{\text{SQC}}(\mathbf{x}_0, \mathbf{p}_0) K_{ii}^{\text{SQC}}(\mathbf{x}_0, \mathbf{p}_0)$ involves the triangle window functions for the n -th and m -th states at time 0. The time-dependent normalization factor $\bar{C}_{nm,kl}(t) \equiv 1$ for $n \neq m$ is also a constant.

The new electronic representation of eq (10) for evaluation of the electronic density matrix at time t , which is denoted as the CPS with triangle window functions (CPS-TW) approach. It has three important properties:

- 1) In the frozen-nuclei limit, the representation of the electronic population-population correlation is exact for the two-state system ($F = 2$) and is expected to be reasonably accurate for the multi-state system ($F \geq 3$). (See more discussion in ref ⁸⁶.)
- 2) The representation of the other three kinds of correlation functions yields the exact frozen-nuclei limit for all cases ($F \geq 2$). (See more discussion in Section S4 of the Supporting Information.)
- 3) Regardless of the approach for dealing with nuclear DOFs, the expression of the electronic population-population correlation (eq (10)) is always positive-definite for all cases ($F \geq 2$).

In comparison to the exact CPS representations of electronic DOFs, the third property (of the CPS-TW approach) is indispensable for solving the negative population problem of phase space mapping dynamics methods for general F -state systems, e.g., as shown in Figures 4 and 7 of ref ⁷³ and in Figure S12 of the Supporting Information of ref ⁸⁴.

By employing the CPS-TW approach instead of the exact CPS representations for electronic DOFs, in addition to using the infinite Wigner coordinate-momentum phase space for nuclear DOFs, we obtain the expression of the correlation function for both electronic and nuclear DOFs

$$\begin{aligned} & \text{Tr}_{n,e} \left[\left(|n\rangle\langle m| \otimes \hat{A}_{nuc} \right) e^{i\hat{H}t} \left(|k\rangle\langle l| \otimes \hat{B}_{nuc} \right) e^{-i\hat{H}t} \right] \\ \mapsto & \left(\bar{C}_{nm,kl}(t) \right)^{-1} (2\pi\hbar)^{-N} \int d\mathbf{R}_0 d\mathbf{P}_0 \int_0^{1-1/F} w(\gamma) d\gamma \int_{S(\mathbf{x}_0, \mathbf{p}_0; \gamma)} F d\mathbf{x}_0 d\mathbf{p}_0 \\ & \times A_W(\mathbf{R}_0, \mathbf{P}_0) B_W(\mathbf{R}_t, \mathbf{P}_t) \bar{G}_{nm,kl}(\mathbf{x}_0, \mathbf{p}_0; \mathbf{x}_t, \mathbf{p}_t) \end{aligned} \quad (21)$$

Here, $\text{Tr}_n [\]$ represents the trace over nuclear DOFs, $A_W(\mathbf{R}, \mathbf{P})$ and $B_W(\mathbf{R}, \mathbf{P})$ are the Wigner phase space functions of nuclear operators \hat{A}_{nuc} and \hat{B}_{nuc} , respectively. For instance,

$A_W(\mathbf{R}, \mathbf{P}) = \int d\Delta \langle \mathbf{R} - \Delta/2 | \hat{A}_{nuc} | \mathbf{R} + \Delta/2 \rangle \exp(-i\Delta \cdot \mathbf{P}/\hbar)$. Provided that eq (21) is the integral expression of the time-dependent property, we propose a new variant of the NaF approach, namely, NaF with triangle window functions (NaF-TW), in the adiabatic representation.

Consider the full Hamiltonian of nuclei and electrons of the system

$$\hat{H} = \frac{1}{2} \hat{\mathbf{P}}^T \mathbf{M}^{-1} \hat{\mathbf{P}} + \hat{H}_{\text{el}}(\hat{\mathbf{R}}) = \frac{1}{2} \hat{\mathbf{P}}^T \mathbf{M}^{-1} \hat{\mathbf{P}} + \sum_k E_k(\mathbf{R}) |\phi_k(\mathbf{R})\rangle \langle \phi_k(\mathbf{R})|, \quad (22)$$

where $\mathbf{M} = \text{diag}\{m_j\}$ is the diagonal nuclear mass matrix, $\hat{H}_{\text{el}}(\hat{\mathbf{R}})$ is the electronic Hamiltonian that includes the kinetic energy of electrons and all the electrostatic potential among electrons and nuclei, and $E_k(\mathbf{R})$ denotes the adiabatic PES of the k -th adiabatic electronic state, $|\phi_k(\mathbf{R})\rangle$. The expression of the right-hand side (RHS) for the full Hamiltonian operator of eq (22) was first employed for phase space mapping methods for non-adiabatic dynamics in refs^{75, 89}. The non-

adiabatic coupling vector in the adiabatic representation is $\mathbf{d}_{mn}(\mathbf{R}) = \left\langle \phi_m(\mathbf{R}) \left| \frac{\partial \phi_n(\mathbf{R})}{\partial \mathbf{R}} \right. \right\rangle$, of which

the J -th component is $d_{mn}^{(J)}(\mathbf{R})$. Note that $-i\mathbf{d}^{(J)}(\mathbf{R})$ is a Hermitian matrix of electronic DOFs

and that vector $-i\mathbf{d}(\mathbf{R})$ implies a non-abelian gauge field^{75, 90}. Assume that $\{|\phi_n\rangle\}$, $n \in \{1, \dots, F\}$

are effectively complete to describe the process and that the gauge field tensor,

$\frac{\partial(-i\mathbf{d}^{(J)})}{\partial R_I} - \frac{\partial(-i\mathbf{d}^{(I)})}{\partial R_J} + i[-i\mathbf{d}^{(I)}, -i\mathbf{d}^{(J)}]_{\text{ele}}$, is close to zero and may be ignored with caution.

Following the procedure for the derivation of NaF in ref⁸⁴, it is straightforward to obtain the EOMs of NaF-TW,

$$\begin{aligned} \dot{\tilde{\mathbf{g}}}(\mathbf{R}) &= -i\mathbf{V}^{(\text{eff})}(\mathbf{R}, \mathbf{P}) \tilde{\mathbf{g}}(\mathbf{R}) \\ \dot{\mathbf{R}} &= \mathbf{M}^{-1} \mathbf{P} \\ \dot{\mathbf{P}} &= \mathbf{f}_{\text{nonadia}}(\mathbf{R}) - \nabla_{\mathbf{R}} E_{J_{\text{occ}}}(\mathbf{R}) \end{aligned}, \quad (23)$$

where $\tilde{\mathbf{g}}(\mathbf{R}) = \tilde{\mathbf{x}}(\mathbf{R}) + i\tilde{\mathbf{p}}(\mathbf{R})$, $(\tilde{\mathbf{x}}, \tilde{\mathbf{p}})$ are electronic mapping variables in the adiabatic representation, \mathbf{P} is the kinematic nuclear momentum of the adiabatic representation^{47, 73, 75, 84} (equivalently, the mapping diabatic momentum^{75, 84}), the elements of the effective potential matrix, $V^{(\text{eff})}$, are functions of nuclear phase space variables,

$$V_{nk}^{(\text{eff})}(\mathbf{R}, \mathbf{P}) = E_n(\mathbf{R})\delta_{nk} - i\mathbf{M}^{-1}\mathbf{P} \cdot \mathbf{d}_{nk}(\mathbf{R}) \quad , \quad (24)$$

and the nonadiabatic nuclear force reads

$$\mathbf{f}_{\text{nonadia}}(\mathbf{R}) = -\sum_{k \neq l} \left[(E_k(\mathbf{R}) - E_l(\mathbf{R})) \mathbf{d}_{lk}(\mathbf{R}) \right] \tilde{\rho}_{kl}(\mathbf{R}) \quad . \quad (25)$$

In eq (25), $\tilde{\rho}_{kl}(\mathbf{R})$ is the element in the k -th row and l -th column of the matrix,

$$\tilde{\rho}(\mathbf{R}) = \frac{(1 + F/3)}{\text{Tr}_e[\tilde{\mathbf{g}}\tilde{\mathbf{g}}^\dagger]} \tilde{\mathbf{g}}\tilde{\mathbf{g}}^\dagger - 1/3 \quad . \quad (26)$$

The $1 + F/3$ term of eq (26) corresponds to the parameter value, $1/3$, suggested in ref⁴⁶. (Please see more discussion in Section S3 of the Supporting Information). The nonadiabatic nuclear force, eq (25) intrinsically accounts for nonadiabatic transition processes in the state-state coupling region and disappears in the region where the state-state coupling vanishes. Its importance in the nuclear EOMs has been demonstrated by the applications to a few benchmark condensed phase model systems⁸⁴. Following ref⁸⁴, the adiabatic nuclear force $-\nabla_{\mathbf{R}} E_{j_{\text{occ}}}(\mathbf{R})$ of eq (23) is contributed from the single-state adiabatic nuclear force that has the largest weight, i.e.,

$$-\sum_k \nabla_{\mathbf{R}} E_k(\mathbf{R}) \left(\prod_{j \neq k} h(\tilde{\rho}_{kk} - \tilde{\rho}_{jj}) \right) \text{ with the Heaviside function } h(y) = \{1 \text{ if } y \geq 0 \text{ else } 0\} \text{ . That is,}$$

the contribution of adiabatic force ingredients with smaller weights is neglected. We focus on this approach of the single-state adiabatic nuclear force from the dominant weight, although other approaches are also possible⁸⁴. The NaF mapping energy (on phase space) in the adiabatic

representation, $H_{\text{NaF}}(\mathbf{R}, \mathbf{P}, \tilde{\mathbf{x}}(\mathbf{R}), \tilde{\mathbf{p}}(\mathbf{R})) \equiv \frac{1}{2} \mathbf{P}^T \mathbf{M}^{-1} \mathbf{P} + E_{j_{\text{occ}}}(\mathbf{R})$, is conserved by rescaling the adiabatic kinematic nuclear momentum \mathbf{P} (that is equivalent to the mapping diabatic momentum^{75, 84}) along the momentum vector after the integration of the EOMs of eq (23) as well as when the largest weight is switched⁸⁴. If it is impossible to conserve the NaF energy when the largest weight is switched, the switching is prohibited, with no change of \mathbf{P} , and the single-state adiabatic nuclear force is still contributed by the gradient of the previously occupied adiabatic PES. The algorithm of NaF-TW is described in detail in Section S1 of the Supporting Information.

We consider a series of typical benchmark condensed phase and gas phase nonadiabatic model systems where numerically exact results are available, which have been used for testing the numerical performance of approximate dynamics methods in refs. ^{73, 75, 84}. The latest SQC approach with triangle window functions of ref⁴⁹ (which is denoted as SQC-TW), the conventional Ehrenfest dynamics³⁰, the fewest-switches surface hopping (FSSH)¹⁶ algorithm described in ref²¹, and the original NaF (with $\gamma = 1/2$) of ref⁸⁴ are also tested for comparison. The initial condition for nuclear DOFs is sampled from the Wigner distribution on nuclear coordinate-momentum phase space, which takes care of nuclear quantum effects in all the trajectory-based nonadiabatic dynamics methods for fair comparison. All simulations are performed in the adiabatic representation. When exact results are available in only the diabatic representation, the diabatic initial condition is transformed to its adiabatic counterpart, and dynamics results in the adiabatic representation are transformed back to the corresponding diabatic results.

We first consider standard system-bath models, where the system is bilinearly coupled with harmonic bath DOFs of a dissipative environment in the condensed phase. The coupling imparts a substantial influence from the bath environment and yields the reduced dynamics of the system across a broad spectrum ranging from coherent to dissipative regimes. Such models serve as

pivotal tools for understanding important processes governing electron/exciton energy transfer dynamics in the realm of chemical and biological reactions. Methodologies that yield numerically exact results for condensed phase system-bath models, most in the diabatic representation, include quasi-adiabatic propagator path integral (QuAPI)⁹¹⁻⁹³ and more efficient small matrix PI (SMatPI)^{94, 95}, hierarchy equations of motion (HEOM)⁹⁶⁻¹⁰⁰, (multi-layer) multi-configuration time-dependent Hartree [(ML-)MCTDH]¹⁰¹⁻¹⁰³, time-dependent density matrix renormalization group (TD-DMRG)¹⁰⁴, and so forth. We use the two-site spin-boson model and the seven-site Fenna–Matthews–Olson (FMO) monomer model for testing trajectory-based nonadiabatic dynamics methods.

Figure 1 investigates four typical spin-boson models at low temperature, which range from weak to strong system-bath coupling. Three hundred discrete bath modes are utilized for the Ohmic spectral density. Initially, the (nuclear) bath DOFs are at thermal equilibrium and the system is in the diabatic excited state. (Please see more numerical details in Section S2-A of the Supporting Information.) In comparison to numerically exact data, while Ehrenfest dynamics produces the worst results, FSSH performs better but does not capture the correct asymptotic behavior for a relatively long time. In contrast, SQC-TW, NaF, and NaF-TW yield results that are in overall good agreement with exact data.

Figure 2 considers the seven-site FMO monomer model related to the photosynthetic organism of green sulfur bacteria. One hundred discrete bath modes per site are employed for the Debye spectral density. At time $t = 0$, the (nuclear) bath DOFs are at thermal equilibrium at 77 K and the first site is occupied. Both Ehrenfest dynamics and FSSH perform poorly even for relatively short time and fail to even qualitatively capture the steady-state behavior in the long-time limit. In comparison, SQC-TW, NaF, and NaF-TW show much better performance and are capable of

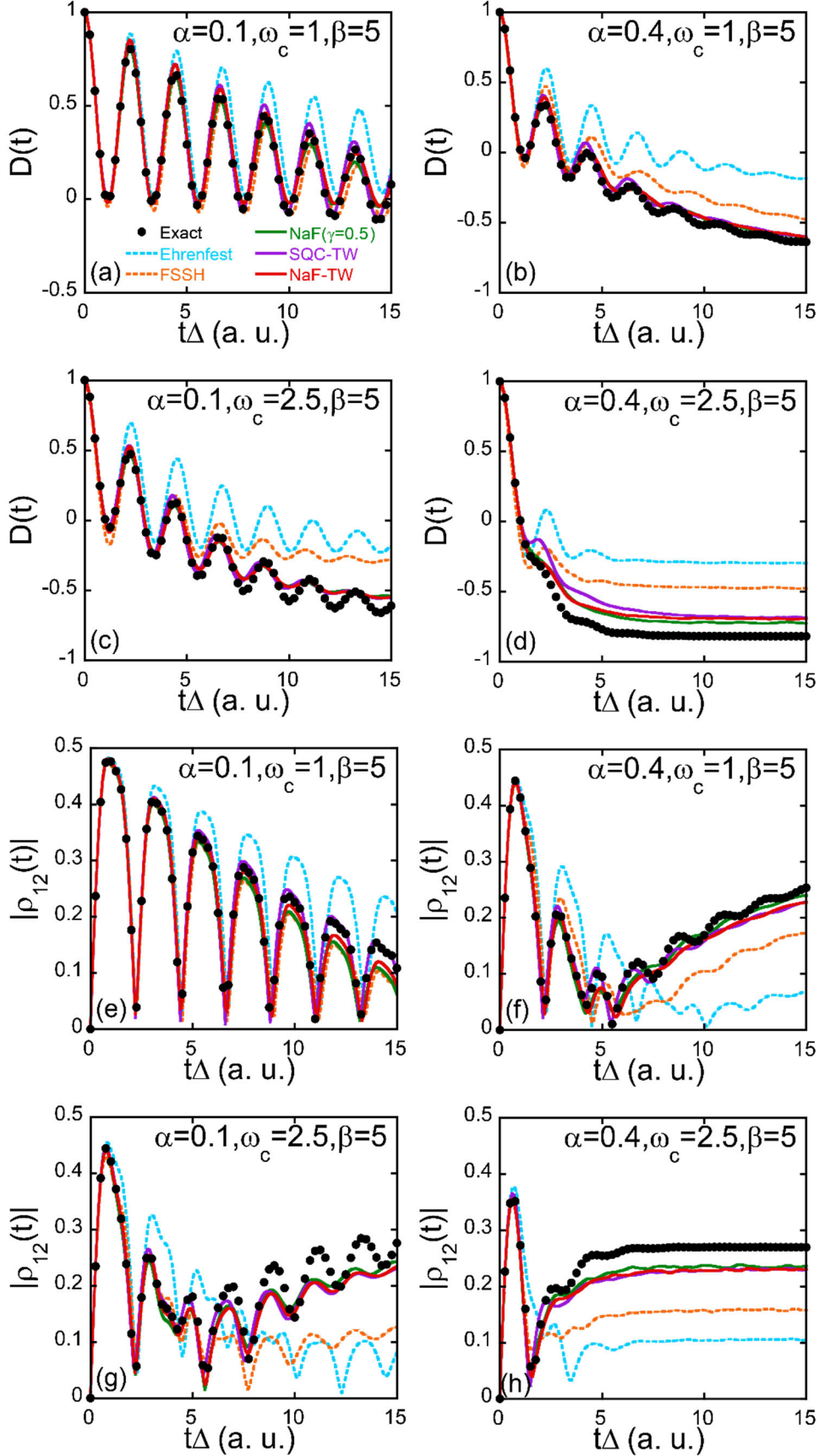


Figure 1. Panels (a-d): The population difference between State 1 and State 2, $D(t)$, as a function of time for the four spin-boson models with the Ohmic spectral density at the inverse temperature $\beta = 5$. Panels (e-h): The modulus of the off-diagonal (coherence) element of the reduced electronic density matrix, $|\rho_{12}(t)|$, as a function of time. Panels (a-d) or (e-h) represent the results of the spin-boson models with parameters $\{\alpha = 0.1, \omega_c = 1\}$, $\{\alpha = 0.4, \omega_c = 1\}$, $\{\alpha = 0.1, \omega_c = 2.5\}$, and $\{\alpha = 0.4, \omega_c = 2.5\}$, respectively. Black points: (exact results produced by) eHEOM. Cyan long-dashed lines: Ehrenfest dynamics. Orange short-dashed lines: FSSH. Green solid lines: NaF. Purple solid lines: SQC-TW. Red solid lines: NaF-TW. Converged results are obtained using three hundred discrete bath modes. For SQC-TW, the expression of the population-population correlation function is equivalent to that of ref⁴⁹ of Cotton and Miller, while eqs (10) and (18)-(19) are used for the population-coherence correlation function because its SQC expression with triangle window functions of ref⁴⁹ is not exact for even the pure two-state system. More details of the parameters of the spin-boson models and the simulations are described in Section S2-A of the Supporting Information.

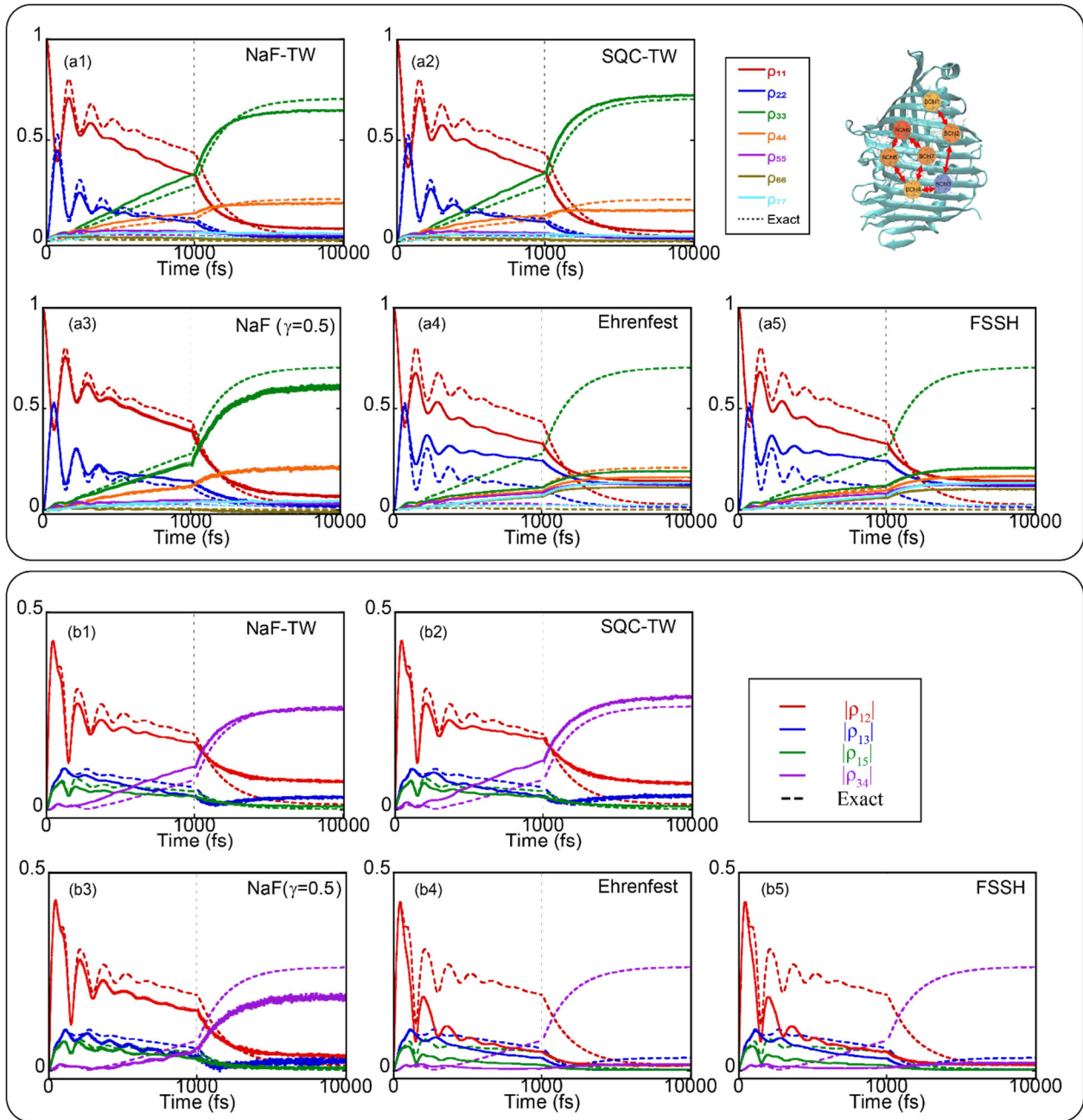


Figure 2. The initially occupied site is Site 1. Panel (a): The population dynamics of the seven-site FMO monomer model at temperature 77 K. The red, blue, green, orange, purple, brown and cyan solid lines represent the population of Sites 1-7, respectively. Panel (b): Dynamics of the off-diagonal (coherence) terms of the reduced electronic density matrix of the same model. The red, blue, green, and purple solid lines illustrate $|\rho_{12}(t)|$, $|\rho_{13}(t)|$, $|\rho_{15}(t)|$ and $|\rho_{34}(t)|$, respectively.

The exact results produced by HEOM are presented by dashed lines in corresponding colors. Sub-panels (a1-a5) or Sub-panels (b1-b5) denote the results of NaF-TW, SQC-TW, NaF($\gamma = 0.5$), Ehrenfest dynamics, and FSSH, respectively. One hundred discrete bath modes for each site are employed to obtain converged results. For SQC-TW, eqs (10) and (18)-(19) are used for the population-coherence correlation function because its SQC expression with triangle window functions for the multi-state system is not available in the literature. More details of the FMO model and the simulations are depicted in Section S2-A of the Supporting Information.

reasonably describing the evolution of both electronic population and “coherence”, from the fast relaxation behavior at short time to the asymptotic behavior at long time.

In either of the two types of system-bath models, the performance of NaF-TW is comparable to that of SQC-TW. This implies that triangle functions for electronic DOFs are not limited to Ehrenfest-like dynamics of the SQC approach, and also work well for NaF dynamics. Both NaF-TW and NaF outperform FSSH, which suggests that the NaF strategy is superior to conventional SH approaches in studying systems where the electronic states remain coupled all the time.

We then consider two typical models of cavity quantum electrodynamics (cQED), where the matter system is tightly coupled to the vacuum field in a confined optical cavity^{10, 105-107}. The first atom-in-cavity model involves two atomic energy levels, and the second one includes three energy levels. The highest energy level is initially occupied. More details of the models and initial conditions are described in Supporting Information S2-B. Figure 3 shows that both Ehrenfest dynamics and FSSH lead to significant deviation since a relatively short time and meet challenges in capturing the re-coherence around $t = 1800$ a.u. In contrast, SQC-TW, NaF, and NaF-TW yield much more accurate data for population dynamics of all energy levels and are capable of semi-

quantitatively describing the short time behavior, as well as the re-absorption and re-emission processes around $t = 1800$ a.u. The comparison between NaF and NaF-TW demonstrates that NaF dynamics performs robustly well, regardless of whether CPS or CPS-TW is used for the electronic representation. The performance of NaF-TW matches, if not exceeds, that of the SQC-TW approach where mean-field trajectories are employed.

The third set of tests focuses on the linear vibronic coupling model (LVCM) that captures the characteristic of the pivotal conical intersection (CI) region of the molecular system in various photo-driven phenomena. We use two LVCMs where MCDTH results in the diabatic representation are available. The first test case involves the two-electronic-state LVCM with three nuclear modes and that with 24 nuclear modes of refs. ^{108, 109}, which mimic the S1/S2 conical intersection of the pyrazine molecule. The initial condition is set as the cross-product of the vibronic ground state and the excited electronically diabatic state (S2) ^{108, 109}. The second test case employs a 3-electronic-state 2-nuclear-mode LVCM of the Cr(CO)₅ molecule, where the initial condition is the cross-product of a Gaussian nuclear wave-packet and the first excited electronically diabatic state as described in ref ¹¹⁰. More details of the LVCMs are demonstrated in Section S2-C of the Supporting Information. Figure 4 shows the results of the population dynamics in all these LVCM cases. FSSH, NaF and NaF-TW significantly outperform Ehrenfest dynamics. While FSSH performs slightly better for the 2-state 24-mode case of pyrazine in Figure 4(b), NaF and NaF-TW are overall superior for the 2-state 3-mode case of pyrazine in Figure 4(a) as well as for the 3-state 2-mode LVCM of the Cr(CO)₅ molecule. NaF-TW considerably improves over SQC-TW for the peaks of long time dynamics of the pyrazine molecule in Figures 4(a-b) and for the population oscillation behavior when the evolution crosses or re-crosses the CI region of the realistic gas phase molecular system as shown in Figures 4(c-e).

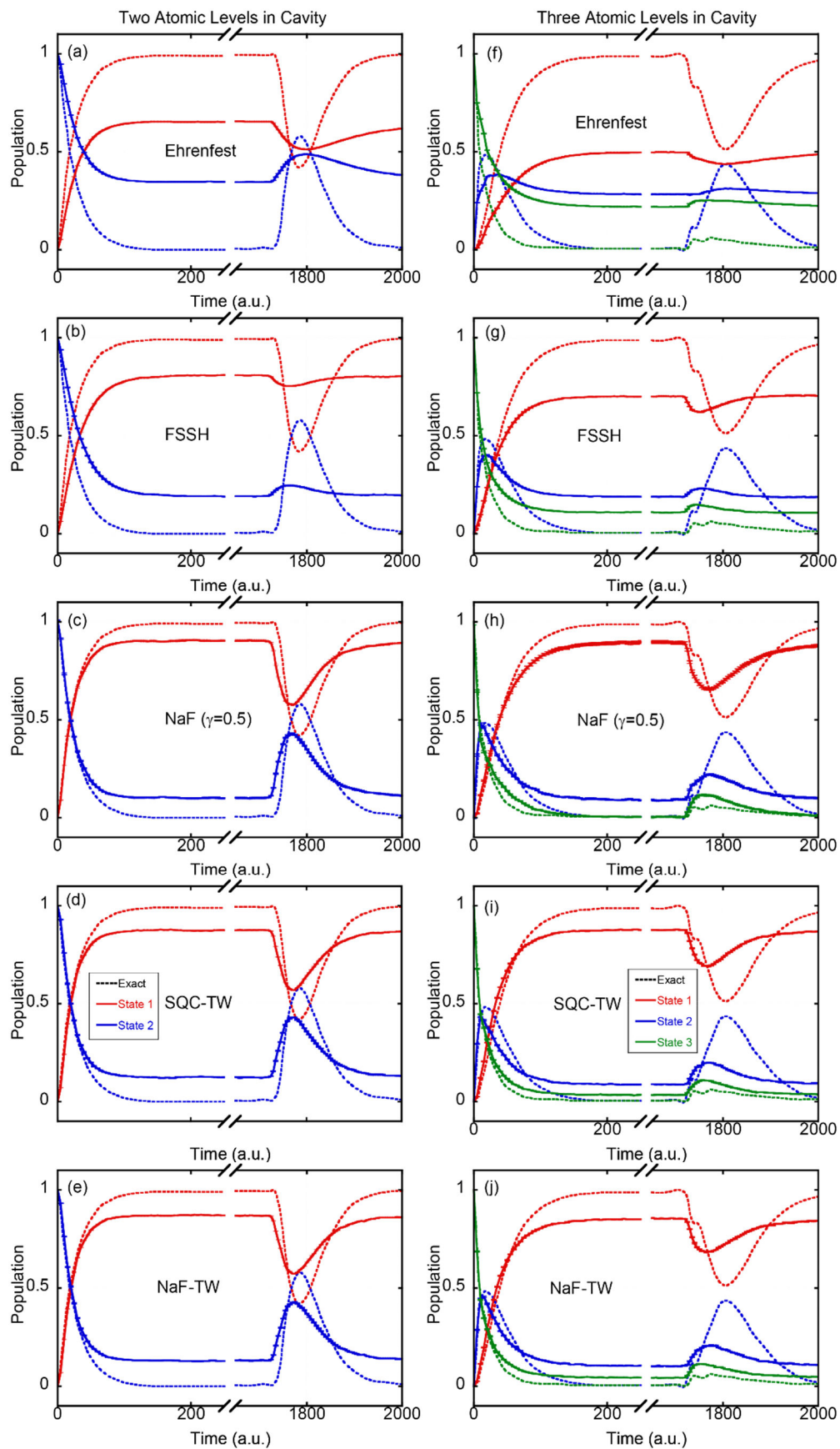


Figure 3. Panels (a-e): Results for the population dynamics of the two-level atom-in-cavity model. The red and blue solid lines represent the population of State 1 and that of State 2, respectively, while the dashed lines in corresponding colors demonstrate the exact results. Panels (f-j): Results of the population dynamics of the three-level atom-in-cavity model. The red, blue and green solid lines represent the population of State 1, State 2 and State 3, respectively, while the dashed lines in corresponding colors demonstrate the exact results. Panels (a-e) or (f-j) present the results of Ehrenfest, FSSH, NaF ($\gamma = 0.5$), SQC-TW, and NaF-TW, respectively. The exact results are obtained from refs ^{111, 112}. Four hundred standing-wave modes for the optical field are used to obtain converged data. More details of the models as well as the simulations are presented in Section S2-B of the Supporting Information.

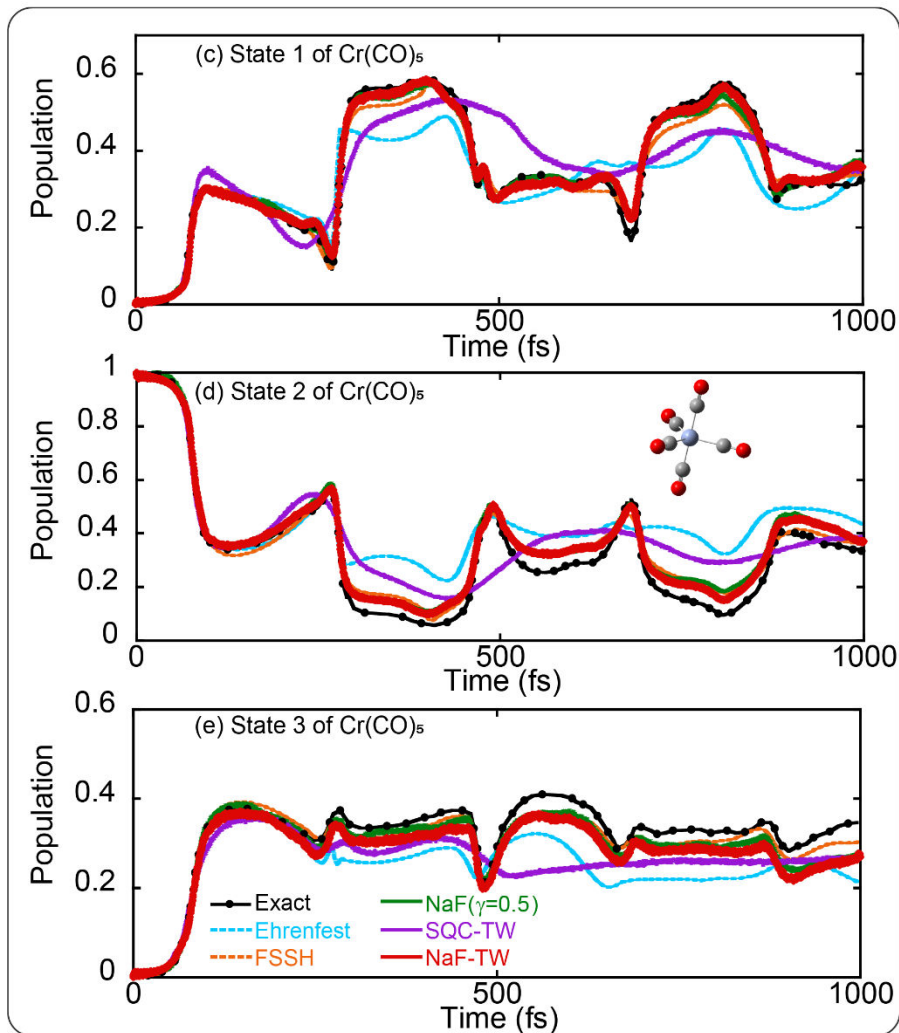
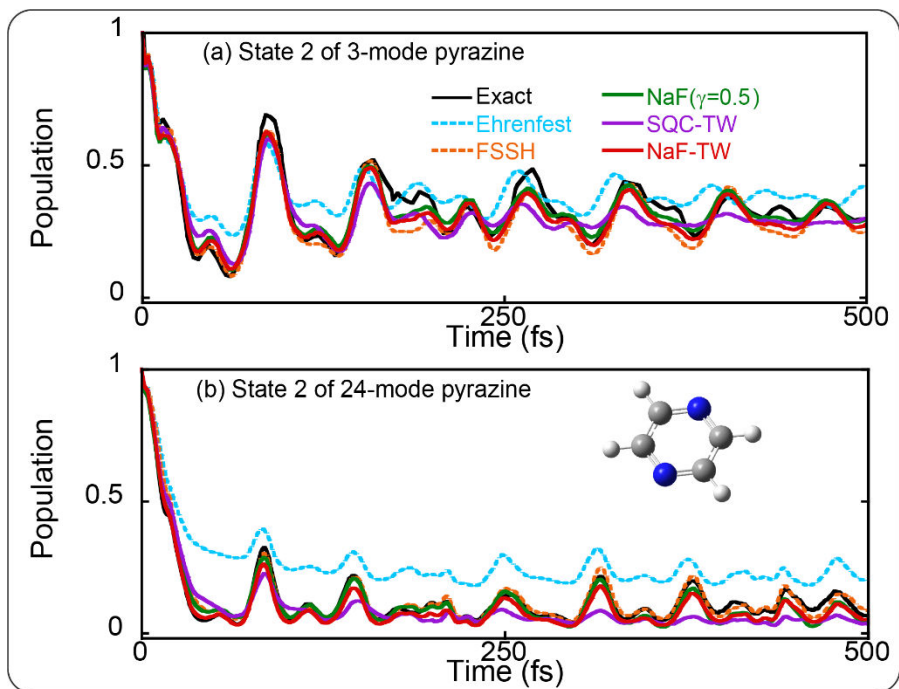


Figure 4. Panels (a-b) denote the population dynamics of the second state of the 2-state LVCM with 3 modes for the pyrazine molecule¹⁰⁸ and that with 24 modes for the same molecule¹⁰⁹, respectively. Panels (c-e) denote the population dynamics of States 1-3 of the 3-state 2-mode LVCM for the Cr(CO)₅ molecule¹¹⁰, respectively. Cyan dashed lines: Ehrenfest dynamics. Orange dashed lines: FSSH. Green solid lines: NaF ($\gamma = 0.5$). Purple solid lines: SQC-TW. Red solid lines: NaF-TW. In Panels (a-b), black solid lines represent exact results produced by MCTDH¹¹³. In Panels (c-e), black solid lines with black points denote exact results obtained from ref¹¹⁰.

Finally, we test typical gas phase models with one anharmonic nuclear DOF where asymptotic regions are involved. The first case includes the coupled three-electronic-state photo-dissociation models of Miller and coworkers³⁸. Numerical details are presented in Section S2-D of the Supporting Information. We focus on Model 3, which is the most challenging. Its nuclear momentum distribution in the long time limit produced by the numerically exact discrete variable representation (DVR) method¹¹⁴ includes one peak in the higher momentum region and another one in the lower momentum region, while that yielded by Ehrenfest dynamics has only one peak and entirely misses the two-peak characteristic in the asymptotic region. Figure 5 demonstrates the results of Model 3. Although SQC-TW noticeably outperforms Ehrenfest dynamics for the electronic population dynamics, it leads to a broader asymptotic nuclear momentum distribution with only one peak. This indicates that SQC-TW with mean field trajectories is not capable of qualitatively capturing the two peaks in the nuclear momentum distribution in the long time limit, which is a consequence of the bifurcation nature of the nuclear motion in the asymptotic region where the nonadiabatic coupling vanishes. As shown in Figure 5, NaF-TW is superior to SQC-

TW and yields results similar to those of FSSH and NaF, which are close to exact data by DVR. The second case involves Tully's standard scattering models¹⁶, among which the extended coupling region (ECR) model is the most challenging one. More details are presented in Section S2-E of the Supporting Information. Quantum dynamics of the ECR model involves both the nuclear wavepacket that transmits forwardly and the one that reflects backwardly in asymptotic regions. The dramatic bifurcation characteristic has considerable influence on both electronic and nuclear dynamics. The performance of Ehrenfest dynamics is poor for the ECR model. Figure 6 shows that SQC-TW improves over Ehrenfest dynamics, but is incompetent in reproducing the sharp step-like change in the transmission/reflection probability on State 2 as a function of the momentum of the center of the initial nuclear gaussian wavepacket. In comparison, NaF-TW, as well as NaF and FSSH, leads to reasonably accurate electronic dynamics for the ECR model. Figure 5(e) and Figure 5(f) demonstrate that, while SQC-TW does not perform well in describing nuclear dynamics for the ECR model, NaF-TW yields a much more accurate nuclear momentum distribution in the asymptotic region in comparison to the exact DVR data. Although NaF-TW and SQC-TW share the same CPS-TW expression of eq (21) for the electronic correlation function, the comparison in Figures 5-6 suggests that NaF dynamics (of NaF-TW) is more consistent than Ehrenfest-like dynamics (of SQC-TW) in describing the correct correlation between electronic and nuclear dynamics.

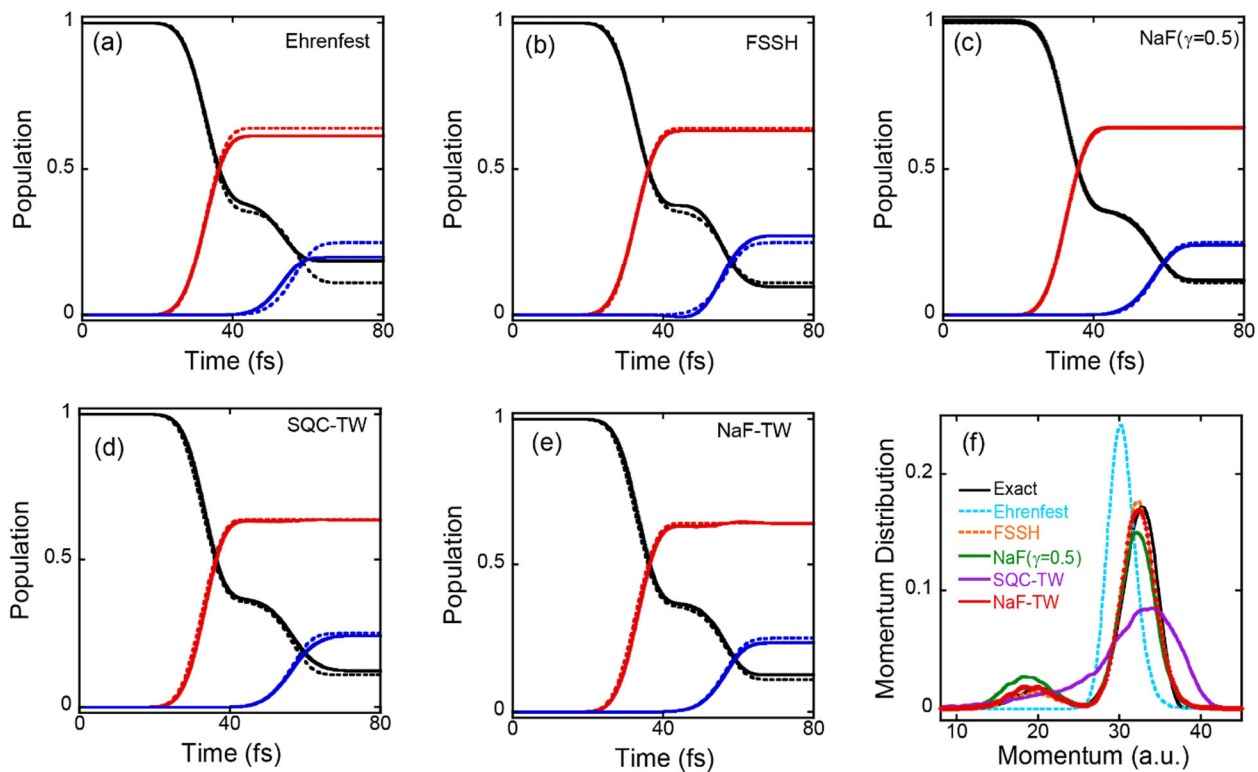


Figure 5. Panels (a-e) denote the population dynamics of the third photo-dissociation model of ref³⁸, where the black, red, and blue solid lines represent the population of States 1-3, respectively, and the exact results produced by DVR are presented by the dashed lines in corresponding colors. Panel (f) presents the nuclear momentum distribution in the asymptotic (long time) limit ($t = 200$ fs), where the cyan dashed, orange dashed, green solid, purple solid, and red solid lines represent the results of Ehrenfest dynamics, FSSH, NaF($\gamma = 0.5$), SQC-TW, and NaF-TW, respectively. The exact nuclear momentum distribution obtained by DVR is presented in the black solid line.

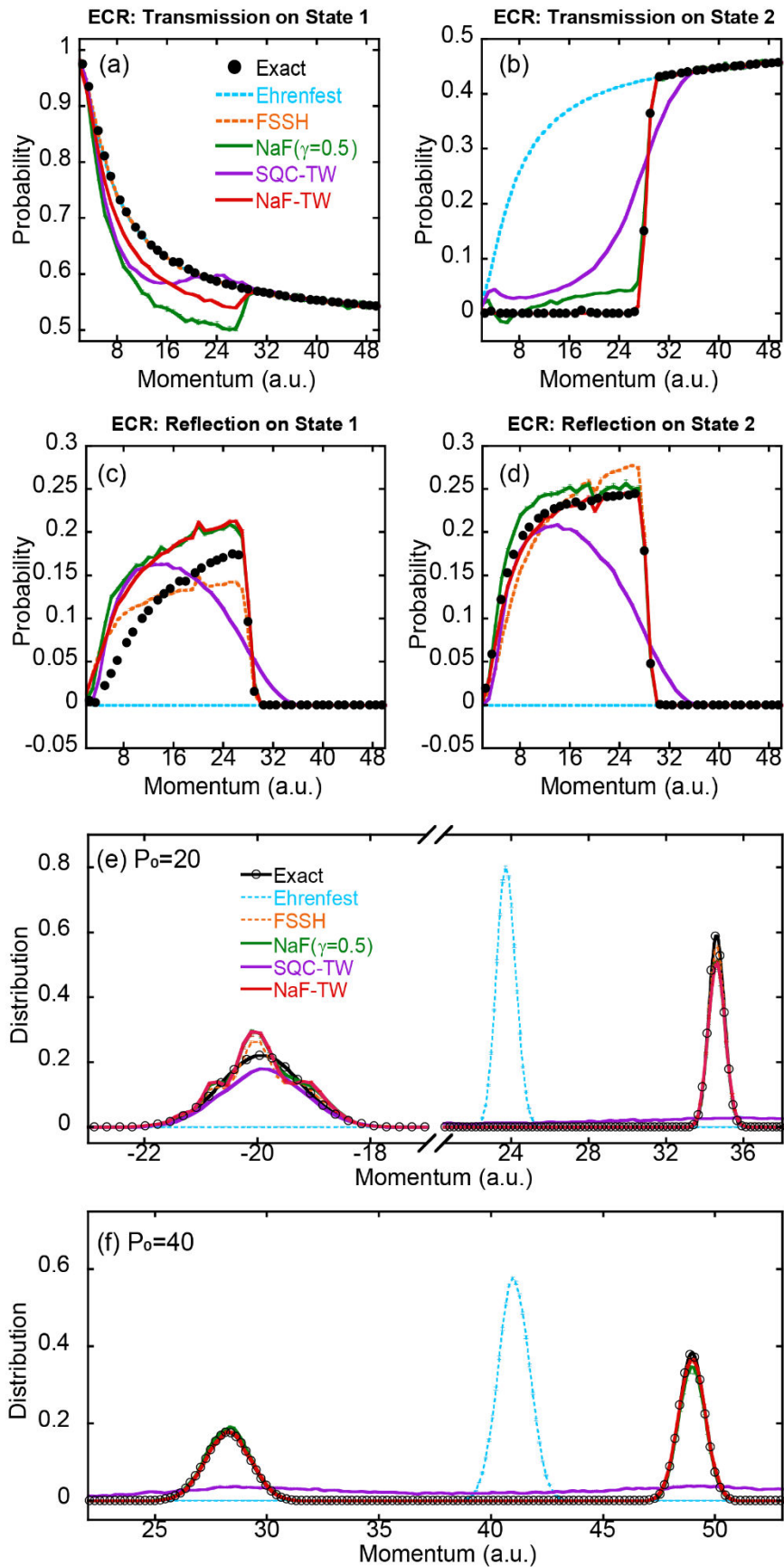


Figure 6. Panels (a-b) denote the transmission probability on (adiabatic) State 1 and that on State 2 for Tully’s ECR model. Panels (c-d) denote the reflection probability on (adiabatic) State 1 and that on State 2 for the same model. Panels (e) and (f) present the asymptotic nuclear momentum distribution for the initial momentum $P_0=20$ of the center of the nuclear Gaussian wavepacket and that for $P_0=40$, respectively. Cyan dashed lines: Ehrenfest dynamics. Orange dashed lines: FSSH. Green solid lines: NaF ($\gamma = 0.5$). Purple solid lines: SQC-TW. Red solid lines: NaF-TW. Black points: Exact results by DVR.

In comparison to the exact CPS formulation for discrete (electronic) DOFs, although the CPS-TW representation of the population-population correlation function (i.e., the population dynamics) is exact for only the pure two-state system⁸⁶, its applications to three-state or multi-state nonadiabatic systems (e.g., in Figures 2, 3(f-j), 4(c-e), and 5) are also reasonably accurate in practice. Because the CPS-TW expression of the population dynamics is always positive-definite irrespective of the number of electronic states and the approximation of nuclear dynamics, the advantage of the CPS-TW representation helps NaF-TW outperform NaF in the cases of Figure 5(f) and Figure 6.

In summary, since the unified phase space formulation with coordinate-momentum variables offers a powerful tool for studying composite systems, we construct the CPS-TW representation for discrete (electronic) DOFs and employ it with the recently developed NaF strategy. It leads to the NaF-TW approach for nonadiabatic transition dynamics. We test the performance of NaF-TW extensively for a series of standard benchmark condensed phase and gas phase nonadiabatic systems where numerically exact data are feasible for comparison. NaF-TW is competent in capturing the dynamical correlation between electronic and nuclear DOFs in a reasonably accurate

manner. The performance of NaF-TW is similar to that of the SQC approach with mean field trajectories⁴⁹ in (molecular) systems where the electronic states remain coupled all the time. More importantly, NaF-TW significantly outperforms the SQC approach in (molecular) systems where the evolution involves the asymptotic region where the state-state coupling disappears. The comprehensive benchmark numerical tests in the main text as well as in the Supporting Information suggest that NaF dynamics is overall superior to conventional surface hopping dynamics and Ehrenfest-like dynamics in a broad region.

Because the CPS formulation and CPS-TW representation can be used for the interpretation of discrete quantum states of light atoms or those of high-frequency vibrational DOFs, the NaF strategy can be employed to study nuclear quantum effects in proton/hydrogen transfer processes^{17, 48, 115}. It is expected that further development of NaF-TW and the CPS formulations “in ever-increasing levels of abstraction” will lead to a promising and robust trajectory-based approach for investigating nonadiabatic transition phenomena and dynamic processes with important quantum effects in complex/large composite systems in chemistry, biology, materials, environmental science, quantum information, quantum computation, and so forth.

■ ASSOCIATED CONTENT

Supporting Information.

Supporting Information is available free of charge via the Internet at the ACS website.

Supporting Information includes five sections: Numerical details for initial sampling and finite time integrator; Simulation details for models in the main text; Comparisons of different NaF-TW strategies; Proof of exact time correlation functions involving coherence terms for pure

multi-electronic-state systems; Alternative phase space formulations derived from triangle window functions. (PDF)

■ AUTHOR INFORMATION

Corresponding Author

*E-mail: jianliupku@pku.edu.cn

ORCID

Xin He: 0000-0002-5189-7204

Xiangsong Cheng: 0000-0001-8793-5092

Baihua Wu: 0000-0002-1256-6859

Jian Liu: 0000-0002-2906-5858

Notes

The authors declare no competing financial interests.

■ ACKNOWLEDGMENT

This work was supported by the National Science Fund for Distinguished Young Scholars Grant No. 22225304. We acknowledge the High-performance Computing Platform of Peking University, Beijing PARATERA Tech Co., Ltd., and Guangzhou supercomputer center for providing computational resources. We thank Youhao Shang, Haocheng Lu, and Bingqi Li for useful discussions. We also thank Bill Miller for having encouraged us to investigate the window function approach.

Reference

1. Polli, D.; Altoe, P.; Weingart, O.; Spillane, K. M.; Manzoni, C.; Brida, D.; Tomasello, G.; Orlandi, G.; Kukura, P.; Mathies, R. A., et al., Conical Intersection Dynamics of the Primary

- Photoisomerization Event in Vision. *Nature* **2010**, *467*, 440-U88. <http://dx.doi.org/10.1038/nature09346>
2. Martinez, T. J., Seaming Is Believing. *Nature* **2010**, *467*, 412-413. <http://dx.doi.org/10.1038/467412a>
 3. Domcke, W.; Yarkony, D. R.; Köppel, H., *Conical Intersections: Theory, Computation and Experiment*. World Scientific: Singapore, 2011.
 4. Scholes, G. D.; Fleming, G. R.; Olaya-Castro, A.; van Grondelle, R., Lessons from Nature About Solar Light Harvesting. *Nat. Chem.* **2011**, *3*, 763-774. <http://dx.doi.org/10.1038/Nchem.1145>
 5. Maiuri, M.; Ostroumov, E. E.; Saer, R. G.; Blankenship, R. E.; Scholes, G. D., Coherent Wavepackets in the Fenna-Matthews-Olson Complex Are Robust to Excitonic-Structure Perturbations Caused by Mutagenesis. *Nat. Chem.* **2018**, *10*, 177-183. <http://dx.doi.org/10.1038/Nchem.2910>
 6. Smith, M. B.; Michl, J., Singlet Fission. *Chem. Rev.* **2010**, *110*, 6891-6936. <http://dx.doi.org/10.1021/cr1002613>
 7. Scholes, G. D.; Rumbles, G., Excitons in Nanoscale Systems. *Nat. Mater.* **2006**, *5*, 683-696. <http://dx.doi.org/10.1038/nmat1710>
 8. Long, R.; Prezhdo, O. V.; Fang, W.-H., Nonadiabatic Charge Dynamics in Novel Solar Cell Materials. *Wiley Interdiscip. Rev. Comput. Mol. Sci.* **2017**, *7*, e1305. <http://dx.doi.org/10.1002/wcms.1305>
 9. Wang, Y.-C.; Ke, Y.; Zhao, Y., The Hierarchical and Perturbative Forms of Stochastic Schrodinger Equations and Their Applications to Carrier Dynamics in Organic Materials. *Wiley Interdiscip. Rev. Comput. Mol. Sci.* **2019**, *9*, e1375. <http://dx.doi.org/10.1002/wcms.1375>
 10. Garcia-Vidal, F. J.; Ciuti, C.; Ebbesen, T. W., Manipulating Matter by Strong Coupling to Vacuum Fields. *Science* **2021**, *373*, eabd0336. <http://dx.doi.org/10.1126/science.abd0336>
 11. Mei, J.; Leung, N. L. C.; Kwok, R. T. K.; Lam, J. W. Y.; Tang, B. Z., Aggregation-Induced Emission: Together We Shine, United We Soar! *Chem. Rev.* **2015**, *115*, 11718-11940. <http://dx.doi.org/10.1021/acs.chemrev.5b00263>
 12. Ye, Z.; Lin, X.; Wang, N.; Zhou, J.; Zhu, M.; Qin, H.; Peng, X., Phonon-Assisted up-Conversion Photoluminescence of Quantum Dots. *Nat. Commun.* **2021**, *12*, 4283. <http://dx.doi.org/10.1038/s41467-021-24560-4>
 13. Xu, Y.; Liang, X.; Zhou, X.; Yuan, P.; Zhou, J.; Wang, C.; Li, B.; Hu, D.; Qiao, X.; Jiang, X., et al., Highly Efficient Blue Fluorescent Oleds Based on Upper Level Triplet-Singlet Intersystem Crossing. *Adv. Mater.* **2019**, *31*, 1807388. <http://dx.doi.org/10.1002/adma.201807388>
 14. Hammes-Schiffer, S., Theoretical Perspectives on Non-Born-Oppenheimer Effects in Chemistry. *Philos. Trans. Royal Soc. A* **2022**, *380*, 20200377. <http://dx.doi.org/10.1098/rsta.2020.0377>
 15. Tully, J. C.; Preston, R. K., Trajectory Surface Hopping Approach to Nonadiabatic Molecular Collisions: The Reaction of H⁺ with D₂. *J. Chem. Phys.* **1971**, *55*, 562-572. <http://dx.doi.org/10.1063/1.1675788>
 16. Tully, J. C., Molecular Dynamics with Electronic Transitions. *J. Chem. Phys.* **1990**, *93*, 1061-1071. <http://dx.doi.org/10.1063/1.459170>
 17. Hammes-Schiffer, S.; Tully, J. C., Proton Transfer in Solution: Molecular Dynamics with Quantum Transitions. *J. Chem. Phys.* **1994**, *101*, 4657-4667. <http://dx.doi.org/10.1063/1.467455>

18. Zhu, C. Y.; Nobusada, K.; Nakamura, H., New Implementation of the Trajectory Surface Hopping Method with Use of the Zhu-Nakamura Theory. *J. Chem. Phys.* **2001**, *115*, 3031-3044. <http://dx.doi.org/10.1063/1.1386811>
19. Craig, C. F.; Duncan, W. R.; Prezhdo, O. V., Trajectory Surface Hopping in the Time-Dependent Kohn-Sham Approach for Electron-Nuclear Dynamics. *Phys. Rev. Lett.* **2005**, *95*, 163001. <http://dx.doi.org/10.1103/physrevlett.95.163001>
20. Wang, L.; Akimov, A.; Prezhdo, O. V., Recent Progress in Surface Hopping: 2011-2015. *J. Phys. Chem. Lett.* **2016**, *7*, 2100-2112. <http://dx.doi.org/10.1021/acs.jpcllett.6b00710>
21. Peng, J.; Xie, Y.; Hu, D.; Du, L.; Lan, Z., Treatment of Nonadiabatic Dynamics by on-the-Fly Trajectory Surface Hopping Dynamics. *Acta Phys.-Chim. Sin.* **2019**, *35*, 28-48. <http://dx.doi.org/10.3866/PKU.WHXB201801042>
22. Barbatti, M., Nonadiabatic Dynamics with Trajectory Surface Hopping Method. *Wiley Interdiscip. Rev. Comput. Mol. Sci.* **2011**, *1*, 620-633. <http://dx.doi.org/10.1002/wcms.64>
23. Tully, J. C., Perspective: Nonadiabatic Dynamics Theory. *J. Chem. Phys.* **2012**, *137*, 22A301. <http://dx.doi.org/10.1063/1.4757762>
24. Granucci, G.; Persico, M.; Spighi, G., Surface Hopping Trajectory Simulations with Spin-Orbit and Dynamical Couplings. *J. Chem. Phys.* **2012**, *137*, 22A501. <http://dx.doi.org/10.1063/1.4707737>
25. Cui, G.; Thiel, W., Generalized Trajectory Surface-Hopping Method for Internal Conversion and Intersystem Crossing. *J. Chem. Phys.* **2014**, *141*, 124101. <http://dx.doi.org/10.1063/1.4894849>
26. Mai, S.; Marquetand, P.; Gonzalez, L., A General Method to Describe Intersystem Crossing Dynamics in Trajectory Surface Hopping. *Int. J. Quantum Chem.* **2015**, *115*, 1215-1231. <http://dx.doi.org/10.1002/qua.24891>
27. Subotnik, J. E.; Jain, A.; Landry, B.; Petit, A.; Ouyang, W.; Bellonzi, N., Understanding the Surface Hopping View of Electronic Transitions and Decoherence. *Annu. Rev. Phys. Chem.* **2016**, *67*, 387-417. <http://dx.doi.org/10.1146/annurev-physchem-040215-112245>
28. Martens, C. C., Surface Hopping by Consensus. *J. Phys. Chem. Lett.* **2016**, *7*, 2610-2615. <http://dx.doi.org/10.1021/acs.jpcllett.6b01186>
29. Kapral, R., Surface Hopping from the Perspective of Quantum-Classical Liouville Dynamics. *Chem. Phys.* **2016**, *481*, 77-83. <http://dx.doi.org/10.1016/j.chemphys.2016.05.016>
30. Ehrenfest, P., Bemerkung über Die Angenäherte Gültigkeit Der Klassischen Mechanik Innerhalb Der Quantenmechanik. *Z. Phys.* **1927**, *45*, 455-457. <http://dx.doi.org/10.1007/BF01329203>
31. Delos, J. B.; Thorson, W. R.; Knudson, S. K., Semiclassical Theory of Inelastic Collisions. I. Classical Picture and Semiclassical Formulation. *Phys. Rev. A* **1972**, *6*, 709-720. <http://dx.doi.org/10.1103/PhysRevA.6.709>
32. Billing, G. D., On the Applicability of the Classical Trajectory Equations in Inelastic Scattering Theory. *Chem. Phys. Lett.* **1975**, *30*, 391-393. [http://dx.doi.org/10.1016/0009-2614\(75\)80014-5](http://dx.doi.org/10.1016/0009-2614(75)80014-5)
33. Micha, D. A., A Self-Consistent Eikonal Treatment of Electronic Transitions in Molecular Collisions. *J. Chem. Phys.* **1983**, *78*, 7138-7145. <http://dx.doi.org/10.1063/1.444753>
34. Meyer, H.-D.; Miller, W. H., A Classical Analog for Electronic Degrees of Freedom in Nonadiabatic Collision Processes. *J. Chem. Phys.* **1979**, *70*, 3214-3223. <http://dx.doi.org/10.1063/1.437910>

35. Sun, X.; Wang, H.; Miller, W. H., Semiclassical Theory of Electronically Nonadiabatic Dynamics: Results of a Linearized Approximation to the Initial Value Representation. *J. Chem. Phys.* **1998**, *109*, 7064-7074. <http://dx.doi.org/10.1063/1.477389>
36. Wang, H.; Song, X.; Chandler, D.; Miller, W. H., Semiclassical Study of Electronically Nonadiabatic Dynamics in the Condensed-Phase: Spin-Boson Problem with Debye Spectral Density. *J. Chem. Phys.* **1999**, *110*, 4828-4840. <http://dx.doi.org/10.1063/1.478388>
37. Stock, G.; Muller, U., Flow of Zero-Point Energy and Exploration of Phase Space in Classical Simulations of Quantum Relaxation Dynamics. *J. Chem. Phys.* **1999**, *111*, 65-76. <http://dx.doi.org/10.1063/1.479254>
38. Coronado, E. A.; Xing, J.; Miller, W. H., Ultrafast Non-Adiabatic Dynamics of Systems with Multiple Surface Crossings: A Test of the Meyer-Miller Hamiltonian with Semiclassical Initial Value Representation Methods. *Chem. Phys. Lett.* **2001**, *349*, 521-529. [http://dx.doi.org/10.1016/s0009-2614\(01\)01242-8](http://dx.doi.org/10.1016/s0009-2614(01)01242-8)
39. Golosov, A. A.; Reichman, D. R., Classical Mapping Approaches for Nonadiabatic Dynamics: Short Time Analysis. *J. Chem. Phys.* **2001**, *114*, 1065-1074. <http://dx.doi.org/10.1063/1.1332812>
40. Bonella, S.; Montemayor, D.; Coker, D. F., Linearized Path Integral Approach for Calculating Nonadiabatic Time Correlation Functions. *Proc. Natl. Acad. Sci.* **2005**, *102*, 6715-6719. <http://dx.doi.org/10.1073/pnas.0408326102>
41. Stock, G.; Thoss, M., Classical Description of Nonadiabatic Quantum Dynamics. In *Adv. Chem. Phys.*, Rice, S. A., Ed. John Wiley and Sons, Inc.: 2005; Vol. 131, pp 243-375.
42. Ananth, N.; Venkataraman, C.; Miller, W. H., Semiclassical Description of Electronically Nonadiabatic Dynamics Via the Initial Value Representation. *J. Chem. Phys.* **2007**, *127*, 084114. <http://dx.doi.org/10.1063/1.2759932>
43. Tao, G.; Miller, W. H., Semiclassical Description of Electronic Excitation Population Transfer in a Model Photosynthetic System. *J. Phys. Chem. Lett.* **2010**, *1*, 891-894. <http://dx.doi.org/10.1021/jz1000825>
44. Huo, P.; Miller, T. F.; Coker, D. F., Communication: Predictive Partial Linearized Path Integral Simulation of Condensed Phase Electron Transfer Dynamics. *J. Chem. Phys.* **2013**, *139*, 151103. <http://dx.doi.org/10.1063/1.4826163>
45. Cotton, S. J.; Miller, W. H., Symmetrical Windowing for Quantum States in Quasi-Classical Trajectory Simulations: Application to Electronically Non-Adiabatic Processes. *J. Chem. Phys.* **2013**, *139*, 234112. <http://dx.doi.org/10.1063/1.4845235>
46. Cotton, S. J.; Miller, W. H., A New Symmetrical Quasi-Classical Model for Electronically Non-Adiabatic Processes: Application to the Case of Weak Non-Adiabatic Coupling. *J. Chem. Phys.* **2016**, *145*, 144108. <http://dx.doi.org/10.1063/1.4963914>
47. Cotton, S. J.; Liang, R.; Miller, W. H., On the Adiabatic Representation of Meyer-Miller Electronic-Nuclear Dynamics. *J. Chem. Phys.* **2017**, *147*, 064112. <http://dx.doi.org/10.1063/1.4995301>
48. Kananenka, A. A.; Hsieh, C. Y.; Cao, J. S.; Geva, E., Nonadiabatic Dynamics Via the Symmetrical Quasi-Classical Method in the Presence of Anharmonicity. *J. Phys. Chem. Lett.* **2018**, *9*, 319-326. <http://dx.doi.org/10.1021/acs.jpcllett.7b03002>
49. Cotton, S. J.; Miller, W. H., Trajectory-Adjusted Electronic Zero Point Energy in Classical Meyer-Miller Vibronic Dynamics: Symmetrical Quasiclassical Application to Photodissociation. *J. Chem. Phys.* **2019**, *150*, 194110. <http://dx.doi.org/10.1063/1.5094458>

50. Cotton, S. J.; Miller, W. H., A Symmetrical Quasi-Classical Windowing Model for the Molecular Dynamics Treatment of Non-Adiabatic Processes Involving Many Electronic States. *J. Chem. Phys.* **2019**, *150*, 104101. <http://dx.doi.org/10.1063/1.5087160>
51. Saller, M. A. C.; Kelly, A.; Richardson, J. O., On the Identity of the Identity Operator in Nonadiabatic Linearized Semiclassical Dynamics. *J. Chem. Phys.* **2019**, *150*, 071101. <http://dx.doi.org/10.1063/1.5082596>
52. Gao, X.; Sailer, M. A. C.; Liu, Y.; Kelly, A.; Richardson, J. O.; Geva, E., Benchmarking Quasiclassical Mapping Hamiltonian Methods for Simulating Electronically Nonadiabatic Molecular Dynamics. *J. Chem. Theory. Comput.* **2020**, *16*, 2883-2895. <http://dx.doi.org/10.1021/acs.jctc.9b01267>
53. Runeson, J. E.; Richardson, J. O., Generalized Spin Mapping for Quantum-Classical Dynamics. *J. Chem. Phys.* **2020**, *152*, 084110. <http://dx.doi.org/10.1063/1.5143412>
54. Saller, M. A. C.; Kelly, A.; Geva, E., Benchmarking Quasiclassical Mapping Hamiltonian Methods for Simulating Cavity-Modified Molecular Dynamics. *J. Phys. Chem. Lett.* **2021**, *12*, 3163-3170. <http://dx.doi.org/10.1021/acs.jpcllett.1c00158>
55. Stock, G.; Thoss, M., Semiclassical Description of Nonadiabatic Quantum Dynamics. *Phys. Rev. Lett.* **1997**, *78*, 578-581. <http://dx.doi.org/10.1103/PhysRevLett.78.578>
56. Liang, R.; Cotton, S. J.; Binder, R.; Hegger, R.; Burghardt, I.; Miller, W. H., The Symmetrical Quasi-Classical Approach to Electronically Nonadiabatic Dynamics Applied to Ultrafast Exciton Migration Processes in Semiconducting Polymers. *J. Chem. Phys.* **2018**, *149*, 044101. <http://dx.doi.org/10.1063/1.5037815>
57. Tang, D.; Fang, W.-H.; Shen, L.; Cui, G., Combining Meyer-Miller Hamiltonian with Electronic Structure Methods for on-the-Fly Nonadiabatic Dynamics Simulations: Implementation and Application. *Phys. Chem. Chem. Phys.* **2019**, *21*, 17109-17117. <http://dx.doi.org/10.1039/c9cp02682g>
58. Peng, J.; Xie, Y.; Hu, D.; Lan, Z., Analysis of Bath Motion in MM-SQC Dynamics Via Dimensionality Reduction Approach: Principal Component Analysis. *J. Chem. Phys.* **2021**, *154*, 094122. <http://dx.doi.org/10.1063/5.0039743>
59. Hu, D.; Xie, Y.; Peng, J.; Lan, Z., On-the-Fly Symmetrical Quasi-Classical Dynamics with Meyer–Miller Mapping Hamiltonian for the Treatment of Nonadiabatic Dynamics at Conical Intersections. *J. Chem. Theory. Comput.* **2021**, *17*, 3267-3279. <http://dx.doi.org/10.1021/acs.jctc.0c01249>
60. Zheng, J.; Peng, J.; Xie, Y.; Long, Y.; Ning, X.; Lan, Z., Study of the Exciton Dynamics in Perylene Bisimide (PBI) Aggregates with Symmetrical Quasiclassical Dynamics Based on the Meyer-Miller Mapping Hamiltonian. *Phys. Chem. Chem. Phys.* **2020**, *22*, 18192-18204. <http://dx.doi.org/10.1039/d0cp00648c>
61. Zheng, J.; Xie, Y.; Jiang, S.; Long, Y.; Ning, X.; Lan, Z., Initial Sampling in Symmetrical Quasiclassical Dynamics Based on Li-Miller Mapping Hamiltonian. *Phys. Chem. Chem. Phys.* **2019**, *21*, 26502-26514. <http://dx.doi.org/10.1039/c9cp03975a>
62. Xie, Y.; Zheng, J.; Lan, Z., Performance Evaluation of the Symmetrical Quasi-Classical Dynamics Method Based on Meyer-Miller Mapping Hamiltonian in the Treatment of Site-Exciton Models. *J. Chem. Phys.* **2018**, *149*, 174105. <http://dx.doi.org/10.1063/1.5047002>
63. Zheng, J.; Xie, Y.; Jiang, S.; Long, Y.; Ning, X.; Lan, Z., Ultrafast Electron Transfer with Symmetrical Quasi-Classical Dynamics Based on Mapping Hamiltonian and Quantum Dynamics Based on MI-Mctdh. *Chinese J. Chem. Phys.* **2017**, *30*, 800-810. <http://dx.doi.org/10.1063/1674-0068/30/cjcp1711210>

64. Hu, Z.; Sun, X., All-Atom Nonadiabatic Semiclassical Mapping Dynamics for Photoinduced Charge Transfer of Organic Photovoltaic Molecules in Explicit Solvents. *J. Chem. Theory. Comput.* **2022**, *18*, 5819-5836. <http://dx.doi.org/10.1021/acs.jctc.2c00631>
65. Hu, Z.; Liu, Z.; Sun, X., Effects of Heterogeneous Protein Environment on Excitation Energy Transfer Dynamics in the Fenna–Matthews–Olson Complex. *J. Phys. Chem. B* **2022**, *126*, 9271-9287. <http://dx.doi.org/10.1021/acs.jpccb.2c06605>
66. Truhlar, D. G., Effective Potentials for Intermediate-Energy Electron Scattering: Testing Theoretical Models. In *Chemical Applications of Atomic and Molecular Electrostatic Potentials*, Politzer, P.; Truhlar, D. G., Eds. Springer US: Boston, MA, 1981; pp 123-172.
67. Yonehara, T.; Takatsuka, K., Phase-Space Averaging and Natural Branching of Nuclear Paths for Nonadiabatic Electron Wavepacket Dynamics. *J. Chem. Phys.* **2008**, *129*, 134109. <http://dx.doi.org/10.1063/1.2987302>
68. Tao, G., Coherence-Controlled Nonadiabatic Dynamics Via State-Space Decomposition: A Consistent Way to Incorporate Ehrenfest and Born-Oppenheimer-Like Treatments of Nuclear Motion. *J. Phys. Chem. Lett.* **2016**, *7*, 4335-4339. <http://dx.doi.org/10.1021/acs.jpcclett.6b01857>
69. Liu, J., A Unified Theoretical Framework for Mapping Models for the Multi-State Hamiltonian. *J. Chem. Phys.* **2016**, *145*, 204105. <http://dx.doi.org/10.1063/1.4967815>
70. Liu, J., Isomorphism between the Multi-State Hamiltonian and the Second-Quantized Many-Electron Hamiltonian with Only 1-Electron Interactions. *J. Chem. Phys.* **2017**, *146*, 024110. <http://dx.doi.org/10.1063/1.4973708>
71. He, X.; Liu, J., A New Perspective for Nonadiabatic Dynamics with Phase Space Mapping Models. *J. Chem. Phys.* **2019**, *151*, 024105. <http://dx.doi.org/10.1063/1.5108736>
72. He, X.; Gong, Z.; Wu, B.; Liu, J., Negative Zero-Point-Energy Parameter in the Meyer-Miller Mapping Model for Nonadiabatic Dynamics. *J. Phys. Chem. Lett.* **2021**, *12*, 2496-2501. <http://dx.doi.org/10.1021/acs.jpcclett.1c00232>
73. He, X.; Wu, B.; Gong, Z.; Liu, J., Commutator Matrix in Phase Space Mapping Models for Nonadiabatic Quantum Dynamics. *J. Phys. Chem. A* **2021**, *125*, 6845-6863. <http://dx.doi.org/10.1021/acs.jpca.1c04429>
74. Liu, J.; He, X.; Wu, B., Unified Formulation of Phase Space Mapping Approaches for Nonadiabatic Quantum Dynamics. *Acc. Chem. Res.* **2021**, *54*, 4215-4228. <http://dx.doi.org/10.1021/acs.accounts.1c00511>
75. He, X.; Wu, B.; Shang, Y.; Li, B.; Cheng, X.; Liu, J., New Phase Space Formulations and Quantum Dynamics Approaches. *Wiley Interdiscip. Rev. Comput. Mol. Sci.* **2022**, *12*, e1619. <http://dx.doi.org/10.1002/wcms.1619>
76. Wu, B.; He, X.; Liu, J., Phase Space Mapping Theory for Nonadiabatic Quantum Molecular Dynamics. In *Volume on Time-Dependent Density Functional Theory: Nonadiabatic Molecular Dynamics*, Zhu, C., Ed. Jenny Stanford Publishing: New York, 2022.
77. Nakahara, M., *Geometry, Topology, and Physics*. 2 ed.; Institute of Physics Publishing: Bristol, 2003.
78. Atiyah, M. F.; Todd, J. A., On Complex Stiefel Manifolds. *Math. Proc. Cambridge Philos. Soc.* **1960**, *56*, 342-353. <http://dx.doi.org/10.1017/s0305004100034642>
79. Shang, Y.; Cheng, X.; Liu, J., **(to be submitted)**.
80. Stratonovich, R. L., On Distributions in Representation Space. *Zh. Eksp. Teor. Fiz.* **1956**, *31*, 1012.

81. Bargueño, P.; Miret–Artés, S., Dissipative and Stochastic Geometric Phase of a Qubit within a Canonical Langevin Framework. *Phys. Rev. A* **2013**, *87*, 012125. <http://dx.doi.org/10.1103/physreva.87.012125>
82. Peñate - Rodríguez, H. C.; Dorta - Urra, A.; Bargueño, P.; Rojas - Lorenzo, G.; Miret - Artés, S., A Langevin Canonical Approach to the Dynamics of Chiral Systems: Populations and Coherences. *Chirality* **2013**, *25*, 514-520. <http://dx.doi.org/10.1002/chir.22155>
83. Peñate - Rodríguez, H. C.; Dorta - Urra, A.; Bargueño, P.; Rojas - Lorenzo, G.; Miret - Artés, S., A Langevin Canonical Approach to the Dynamics of Chiral Systems: Thermal Averages and Heat Capacity. *Chirality* **2014**, *26*, 319-325. <http://dx.doi.org/10.1002/chir.22326>
84. Wu, B.; He, X.; Liu, J., Nonadiabatic Field on Quantum Phase Space: A Century after Ehrenfest. *J. Phys. Chem. Lett.* **2024**, *15*, 644-658. <http://dx.doi.org/10.1021/acs.jpcllett.3c03385>
85. Lang, H.; Vendrell, O.; Hauke, P., Generalized Discrete Truncated Wigner Approximation for Nonadiabatic Quantum-Classical Dynamics. *J. Chem. Phys.* **2021**, *155*, 024111. <http://dx.doi.org/10.1063/5.0054696>
86. Cheng, X.; He, X.; Liu, J., A Novel Class of Phase Space Representations for Exact Population Dynamics of Two-State Quantum Systems. *Chinese J. Chem. Phys.* **submitted**.
87. Shang, Y. On Quantum Phase Space Mapping Theory and Trajectory-Based Dynamics Approaches. B. S. Thesis, (Advisor: Liu, J.), Peking University, China, 2022.
88. Miller, W. H.; Cotton, S. J., Communication: Wigner Functions in Action-Angle Variables, Bohr-Sommerfeld Quantization, the Heisenberg Correspondence Principle, and a Symmetrical Quasi-Classical Approach to the Full Electronic Density Matrix. *J. Chem. Phys.* **2016**, *145*, 081102. <http://dx.doi.org/10.1063/1.4961551>
89. Lang, H. Quantum Dynamics of Chemical Systems with Large Number of Degrees of Freedom: Linearized Phase Space Methods and Quantum Simulations. Ph.D. Dissertation, (Advisor: Ruprecht Karl University of Heidelberg, Heidelberg, Baden-Württemberg, Germany, 2022.
90. Das, A., *Field Theory*. World Scientific: Singapore, 2019.
91. Makarov, D. E.; Makri, N., Path Integrals for Dissipative Systems by Tensor Multiplication. Condensed Phase Quantum Dynamics for Arbitrarily Long Time. *Chem. Phys. Lett.* **1994**, *221*, 482-491. [http://dx.doi.org/10.1016/0009-2614\(94\)00275-4](http://dx.doi.org/10.1016/0009-2614(94)00275-4)
92. Makri, N.; Makarov, D. E., Tensor Propagator for Iterative Quantum Time Evolution of Reduced Density Matrices. II. Numerical Methodology. *J. Chem. Phys.* **1995**, *102*, 4611-4618. <http://dx.doi.org/10.1063/1.469509>
93. Makri, N.; Makarov, D. E., Tensor Propagator for Iterative Quantum Time Evolution of Reduced Density Matrices. I. Theory. *J. Chem. Phys.* **1995**, *102*, 4600-4610. <http://dx.doi.org/10.1063/1.469508>
94. Makri, N., Small Matrix Path Integral with Extended Memory. *J. Chem. Theory. Comput.* **2021**, *17*, 1-6. <http://dx.doi.org/10.1021/acs.jctc.0c00987>
95. Makri, N., Small Matrix Disentanglement of the Path Integral: Overcoming the Exponential Tensor Scaling with Memory Length. *J. Chem. Phys.* **2020**, *152*, 041104. <http://dx.doi.org/10.1063/1.5139473>
96. Tanimura, Y.; Kubo, R., Time Evolution of a Quantum System in Contact with a Nearly Gaussian-Markoffian Noise Bath. *J. Phys. Soc. Jpn.* **1989**, *58*, 101-114. <http://dx.doi.org/10.1143/JPSJ.58.101>

97. Yan, Y.-A.; Yang, F.; Liu, Y.; Shao, J., Hierarchical Approach Based on Stochastic Decoupling to Dissipative Systems. *Chem. Phys. Lett.* **2004**, *395*, 216-221. <http://dx.doi.org/10.1016/j.cplett.2004.07.036>
98. Xu, R.-X.; Cui, P.; Li, X.-Q.; Mo, Y.; Yan, Y., Exact Quantum Master Equation Via the Calculus on Path Integrals. *J. Chem. Phys.* **2005**, *122*, 041103. <http://dx.doi.org/10.1063/1.1850899>
99. Shao, J., Stochastic Description of Quantum Open Systems: Formal Solution and Strong Dissipation Limit. *Chem. Phys.* **2006**, *322*, 187-192. <http://dx.doi.org/10.1016/j.chemphys.2005.08.007>
100. Moix, J. M.; Cao, J., A Hybrid Stochastic Hierarchy Equations of Motion Approach to Treat the Low Temperature Dynamics of Non-Markovian Open Quantum Systems. *J. Chem. Phys.* **2013**, *139*, 134106. <http://dx.doi.org/10.1063/1.4822043>
101. Meyer, H.-D.; Manthe, U.; Cederbaum, L. S., The Multi-Configurational Time-Dependent Hartree Approach. *Chem. Phys. Lett.* **1990**, *165*, 73-78. [http://dx.doi.org/10.1016/0009-2614\(90\)87014-i](http://dx.doi.org/10.1016/0009-2614(90)87014-i)
102. Thoss, M.; Wang, H.; Miller, W. H., Self-Consistent Hybrid Approach for Complex Systems: Application to the Spin-Boson Model with Debye Spectral Density. *J. Chem. Phys.* **2001**, *115*, 2991-3005. <http://dx.doi.org/10.1063/1.1385562>
103. Wang, H.; Thoss, M., Multilayer Formulation of the Multiconfiguration Time-Dependent Hartree Theory. *J. Chem. Phys.* **2003**, *119*, 1289-1299. <http://dx.doi.org/10.1063/1.1580111>
104. Ren, J. J.; Li, W. T.; Jiang, T.; Wang, Y. H.; Shuai, Z. G., Time-Dependent Density Matrix Renormalization Group Method for Quantum Dynamics in Complex Systems. *Wiley Interdiscip. Rev. Comput. Mol. Sci.* **2022**, *12*, e1614. <http://dx.doi.org/10.1002/wcms.1614>
105. Haugland, T. S.; Ronca, E.; Kjørstad, E. F.; Rubio, A.; Koch, H., Coupled Cluster Theory for Molecular Polaritons: Changing Ground and Excited States. *Phys. Rev. X* **2020**, *10*, 041043. <http://dx.doi.org/10.1103/PhysRevX.10.041043>
106. Toida, H.; Nakajima, T.; Komiyama, S., Vacuum Rabi Splitting in a Semiconductor Circuit Qed System. *Phys. Rev. Lett.* **2013**, *110*, 066802. <http://dx.doi.org/10.1103/PhysRevLett.110.066802>
107. Guerin, W.; Santo, T.; Weiss, P.; Cipris, A.; Schachenmayer, J.; Kaiser, R.; Bachelard, R., Collective Multimode Vacuum Rabi Splitting. *Phys. Rev. Lett.* **2019**, *123*, 243401. <http://dx.doi.org/10.1103/PhysRevLett.123.243401>
108. Schneider, R.; Domcke, W., S1-S2 Conical Intersection and Ultrafast S2->S1 Internal Conversion in Pyrazine. *Chem. Phys. Lett.* **1988**, *150*, 235-242. [http://dx.doi.org/10.1016/0009-2614\(88\)80034-4](http://dx.doi.org/10.1016/0009-2614(88)80034-4)
109. Krempl, S.; Winterstetter, M.; Plöhn, H.; Domcke, W., Path-Integral Treatment of Multi-Mode Vibronic Coupling. *J. Chem. Phys.* **1994**, *100*, 926-937. <http://dx.doi.org/10.1063/1.467253>
110. Worth, G. A.; Welch, G.; Paterson, M. J., Wavepacket Dynamics Study of Cr(CO)₅ after Formation by Photodissociation: Relaxation through an (E ⊕ A) ⊗ e Jahn–Teller Conical Intersection. *Mol. Phys.* **2006**, *104*, 1095-1105. <http://dx.doi.org/10.1080/00268970500418182>
111. Hoffmann, N. M.; Schafer, C.; Rubio, A.; Kelly, A.; Appel, H., Capturing Vacuum Fluctuations and Photon Correlations in Cavity Quantum Electrodynamics with Multitrajectory Ehrenfest Dynamics. *Phys. Rev. A* **2019**, *99*, 063819. <http://dx.doi.org/10.1103/PhysRevA.99.063819>
112. Hoffmann, N. M.; Schäfer, C.; Säkkinen, N.; Rubio, A.; Appel, H.; Kelly, A., Benchmarking Semiclassical and Perturbative Methods for Real-Time Simulations of Cavity-

Bound Emission and Interference. *J. Chem. Phys.* **2019**, *151*, 244113. <http://dx.doi.org/10.1063/1.5128076>

113. Worth, G. A.; Beck, M. H.; Jackle, A.; Meyer, H.-D. The MCTDH Package, Version 8.2, (2000). H.-D. Meyer, Version 8.3 (2002), Version 8.4 (2007). O. Vendrell and H.-D. Meyer Version 8.5 (2013). Version 8.5 contains the ML-MCTDH algorithm. See <http://mctdh.uni-hd.de>. (accessed on November 1st, 2023) Used version: 8.5.14.

114. Colbert, D. T.; Miller, W. H., A Novel Discrete Variable Representation for Quantum Mechanical Reactive Scattering Via the S-Matrix Kohn Method. *J. Chem. Phys.* **1992**, *96*, 1982-1991. <http://dx.doi.org/10.1063/1.462100>

115. Topaler, M.; Makri, N., Quantum Rates for a Double Well Coupled to a Dissipative Bath: Accurate Path Integral Results and Comparison with Approximate Theories. *J. Chem. Phys.* **1994**, *101*, 7500-7519. <http://dx.doi.org/10.1063/1.468244>

Supporting Information:

Nonadiabatic Field with Triangle Window

Functions on Quantum Phase Space

*Xin He, Xiangsong Cheng, Baihua Wu, and Jian Liu**

Beijing National Laboratory for Molecular Sciences, Institute of Theoretical and Computational
Chemistry, College of Chemistry and Molecular Engineering,
Peking University, Beijing 100871, China

AUTHOR INFORMATION

Corresponding Author

* Electronic mail: jianliupku@pku.edu.cn

S1: Numerical Details

Within the phase space framework, the trajectory-based quantum dynamics methods for nonadiabatic systems feature three key aspects: the initial condition, the time correlation function, and the equations of motion of trajectories. The main text of this paper introduces NaF-TW dynamics, which employs the triangle window (TW) functions for the time correlation functions. This feature makes NaF-TW dynamics distinguished from the original NaF dynamics. In this section, we present the numerical details of NaF-TW dynamics, NaF dynamics, and SQC-TW dynamics.

S1-A: Initial Conditions for NaF-TW, NaF and SQC-TW Dynamics

In NaF dynamics, the initial values of electronic phase space variables, $(\mathbf{x}(0), \mathbf{p}(0))$ in the diabatic representation or $(\tilde{\mathbf{x}}(0), \tilde{\mathbf{p}}(0))$ in the adiabatic representation, are uniformly sampled on the CPS, which is the $2F$ -dimensional sphere corresponding to $\mathcal{S}(\mathbf{x}, \mathbf{p}; \gamma)$. In NaF-TW or SQC-TW dynamics, the initial values of electronic phase space variables, $(\mathbf{x}(0), \mathbf{p}(0))$ in the diabatic representation (and similarly for $(\tilde{\mathbf{x}}(0), \tilde{\mathbf{p}}(0))$ in the adiabatic representation), are sampled from the quantized submanifold $\mathcal{M}_{j_{\text{occ}}}$ according the following procedure. We define the action variables $\{\mathbf{e}\}$ and angle variables $\{\boldsymbol{\theta}\}$ as

$$\begin{aligned} e^{(k)} &= \frac{1}{2} \left((x^{(k)})^2 + (p^{(k)})^2 \right) \\ \theta^{(k)} &= \arctan(p^{(k)} / x^{(k)}) \end{aligned} \quad (\text{S1})$$

The initial values of $\{e_0^{(k)}, k = 1, \dots, F\}$ are sampled via Cotton's algorithm which is described in ref¹, and those of $\{\theta_0^{(k)}, k = 1, \dots, F\}$ are uniformly sampled on $[0, 2\pi)$. The sampled $(\mathbf{e}(0), \boldsymbol{\theta}(0))$ is then transformed back to $(\mathbf{x}(0), \mathbf{p}(0))$ according to eq (S1).

The NaF-TW, NaF, and SQC-TW dynamics also vary in their treatment of the initial condition of the commutator matrix $\Gamma(0)$ in the diabatic representation (or $\tilde{\Gamma}(0)$ in the adiabatic representation). For NaF-TW dynamics in the main text, $\Gamma(0)$ (or $\tilde{\Gamma}(0)$) is set to $\gamma\mathbf{I}$, termed the scalar approach. Meanwhile, for NaF dynamics and SQC-TW dynamics, the initial commutator matrix is given by

$$\Gamma_{nm}(0) = \left(\frac{1}{2} \left((x^{(n)}(0))^2 + (p^{(n)}(0))^2 \right) - \delta_{n,j_{\text{occ}}} \right) \delta_{nm} \quad (\text{S2})$$

in the diabatic representation, or

$$\tilde{\Gamma}_{nm}(0) = \left(\frac{1}{2} \left((\tilde{x}^{(n)}(0))^2 + (\tilde{p}^{(n)}(0))^2 \right) - \delta_{n,j_{\text{occ}}} \right) \delta_{nm} \quad (\text{S3})$$

in the adiabatic representation. This approach is referred to as the full commutator matrix approach. As mentioned in the main text, when the initial sampling is done in the diabatic representation, the phase space variables $(\mathbf{x}(0), \mathbf{p}(0))$ as well as the commutator matrix $\Gamma(0)$ are transformed to the adiabatic representation in order to perform the NaF dynamics.

S1-B: Numerical Integrator for Trajectory Dynamics

Numerical Integrator for NaF-TW and NaF

Numerical integrators are employed in the realization of NaF and NaF-TW dynamics. There are six steps in one time step Δt , updating the nuclear coordinates \mathbf{R} , kinematic momentum \mathbf{P} ,

electronic phase variables $\tilde{\mathbf{g}} = \tilde{\mathbf{x}} + i\tilde{\mathbf{p}}$, and commutator matrix $\tilde{\Gamma}$ in the adiabatic representation. In this part, we describe the six steps in details.

Step 1: Propagate the nuclear kinematic momentum within half a time step $\Delta t/2$

$$\mathbf{P}_{t+\Delta t/2} \leftarrow \mathbf{P}_t + \left(-\nabla_{\mathbf{R}} E_{j_{\text{occ}}}(t)(\mathbf{R}_t) + \mathbf{f}_{\text{nonadia}}(t) \right) \frac{\Delta t}{2}, \quad (\text{S4})$$

where $-\nabla_{\mathbf{R}} E_{j_{\text{occ}}}(\mathbf{R}_t)$ represents the state-specific force evolving on the $j_{\text{occ}}(t)$ -th state, and

$\mathbf{f}_{\text{nonadia}}(t) = -\sum_{k \neq l} \left[(E_k(\mathbf{R}_t) - E_l(\mathbf{R}_t)) \mathbf{d}_{lk}(\mathbf{R}_t) \right] \tilde{\rho}_{kl}(t)$ stands for the state-dependent nonadiabatic

force. Here $\tilde{\rho}(t)$ denotes the quasi-density matrix, which is

$$\tilde{\rho}(t) = \frac{1}{2} \tilde{\mathbf{g}}(t) \tilde{\mathbf{g}}^\dagger(t) - \tilde{\Gamma}(t) \quad (\text{S5})$$

for NaF, and

$$\tilde{\rho}(t) = (1 + F/3) \tilde{\mathbf{g}}(t) \tilde{\mathbf{g}}^\dagger(t) / \text{Tr}_e \left[\tilde{\mathbf{g}}(t) \tilde{\mathbf{g}}^\dagger(t) \right] - \mathbf{1}/3 \quad (\text{S6})$$

for NaF-TW.

Step 2: Propagate the nuclear coordinate within a full time step Δt

$$\mathbf{R}_{t+\Delta t} \leftarrow \mathbf{R}_t + \mathbf{M}^{-1} \mathbf{P}_{t+\Delta t/2} \Delta t. \quad (\text{S7})$$

Step 3: Propagate phase variables of electronic DOFs within a full time step Δt according to

$$\tilde{\mathbf{g}}_{t+\Delta t} \leftarrow \tilde{\mathbf{U}}(\mathbf{R}_{t+\Delta t}, \mathbf{P}_{t+\Delta t/2}; \Delta t) \tilde{\mathbf{g}}_t. \quad (\text{S8})$$

Here, $\tilde{\mathbf{U}}(\mathbf{R}(t), \mathbf{P}(t); \Delta t) = \exp \left[-i \Delta t \mathbf{V}^{(\text{eff})}(\mathbf{R}(t), \mathbf{P}(t)) \right]$ denotes the unitary short time propagator within a full-time step Δt in the adiabatic representation. Moreover, in the case of NaF, the

equation of motion for $\tilde{\Gamma}$ reads $\dot{\tilde{\Gamma}} = i[\tilde{\Gamma} \mathbf{V}^{(\text{eff})}(\mathbf{R}, \mathbf{P}) - \mathbf{V}^{(\text{eff})}(\mathbf{R}, \mathbf{P}) \tilde{\Gamma}]$, leading to the propagator within a full time step,

$$\tilde{\Gamma}_{t+\Delta t} \leftarrow \tilde{\mathbf{U}}(\mathbf{R}_{t+\Delta t}, \mathbf{P}_{t+\Delta t/2}; \Delta t) \tilde{\Gamma}_t \tilde{\mathbf{U}}^\dagger(\mathbf{R}_{t+\Delta t}, \mathbf{P}_{t+\Delta t/2}; \Delta t). \quad (\text{S9})$$

In cases where it is more convenient to utilize potential energy surfaces in the diabatic representation, the short time propagator in the adiabatic representation can be replaced with $\mathbf{T}^\dagger(\mathbf{R}_{t+\Delta t}) \exp[-i\Delta t \mathbf{V}(\mathbf{R}_{t+\Delta t})] \mathbf{T}(\mathbf{R}_t)$, where $\mathbf{T}(\mathbf{R})$ represents the diabatic-to-adiabatic transformation matrix with elements $T_{nm}(\mathbf{R}) = \langle n | \phi_m(\mathbf{R}) \rangle$ and $\mathbf{V}(\mathbf{R})$ denotes the diabatic potential energy surfaces matrix.

Step 4: Update $j_{\text{occ}}(t)$ to a new occupied state $j_{\text{occ}}(t + \Delta t)$ based on the switching strategy, i.e., select the state with the largest weight. Following this, rescale \mathbf{P} if $j_{\text{occ}}(t + \Delta t) \neq j_{\text{occ}}(t)$,

$$\mathbf{P}_{t+\Delta t/2} \leftarrow \mathbf{P}_{t+\Delta t/2} \sqrt{\frac{H_{\text{NaF}}(\mathbf{R}_{t+\Delta t}, \mathbf{P}_{t+\Delta t/2}, \tilde{\mathbf{x}}_{t+\Delta t}, \tilde{\mathbf{p}}_{t+\Delta t}) - E_{j_{\text{occ}}(t+\Delta t)}(\mathbf{R}_{t+\Delta t})}{\mathbf{P}_{t+\Delta t/2}^T \mathbf{M}^{-1} \mathbf{P}_{t+\Delta t/2} / 2}}. \quad (\text{S10})$$

If $H_{\text{NaF}}(\mathbf{R}_{t+\Delta t}, \mathbf{P}_{t+\Delta t/2}, \tilde{\mathbf{x}}_{t+\Delta t}, \tilde{\mathbf{p}}_{t+\Delta t}) < E_{j_{\text{occ}}(t+\Delta t)}(\mathbf{R}_{t+\Delta t})$, the switching of the adiabatic nuclear force component is frustrated. In such a case we keep $j_{\text{occ}}(t + \Delta t) = j_{\text{occ}}(t)$ and the rescaling step eq (S10) is skipped.

Step 5: Propagate the nuclear kinematic momentum within the other half time step $\Delta t/2$

$$\mathbf{P}_{t+\Delta t} \leftarrow \mathbf{P}_{t+\Delta t/2} + \left(-\nabla_{\mathbf{R}} E_{j_{\text{occ}}(t+\Delta t)}(\mathbf{R}_{t+\Delta t}) + \mathbf{f}_{\text{nonadia}}(t + \Delta t) \right) \frac{\Delta t}{2}. \quad (\text{S11})$$

Step 6: Finally, rescale the nuclear kinematic momentum \mathbf{P} again to ensure energy conservation in the mapping variables:

$$\mathbf{P}_{t+\Delta t} \leftarrow \mathbf{P}_{t+\Delta t} \sqrt{\frac{H_{\text{NaF}}(\mathbf{R}_0, \mathbf{P}_0, \tilde{\mathbf{x}}_0, \tilde{\mathbf{p}}_0) - E_{j_{\text{occ}}(t+\Delta t)}(\mathbf{R}_{t+\Delta t})}{\mathbf{P}_{t+\Delta t}^T \mathbf{M}^{-1} \mathbf{P}_{t+\Delta t} / 2}}. \quad (\text{S12})$$

If $H_{\text{NaF}}(\mathbf{R}_0, \mathbf{P}_0, \tilde{\mathbf{x}}_0, \tilde{\mathbf{p}}_0) < E_{j_{\text{occ}}(t+\Delta t)}(\mathbf{R}_{t+\Delta t})$, it indicates that the time step size Δt is relatively large for the integrator from time t to time $t + \Delta t$. In such a case, one should then choose a smaller time step size Δt and repeat Steps 1-6 for the update of $(\mathbf{R}_{t+\Delta t}, \mathbf{P}_{t+\Delta t}, \tilde{\mathbf{x}}_{t+\Delta t}, \tilde{\mathbf{p}}_{t+\Delta t})$ from $(\mathbf{R}_t, \mathbf{P}_t, \tilde{\mathbf{x}}_t, \tilde{\mathbf{p}}_t)$. The time step size Δt should be adjusted in the region where the sum of adiabatic and nonadiabatic nuclear force terms is large.

The rescaling of \mathbf{P} alongside its direction is used in the numerical propagators in order to ensure the energy conservation. In similar virtue, in Steps 1 and 5, $\mathbf{f}_{\text{nonadia}}$ of eq (S4) and eq (S11) can also be replaced by its projected component $\mathbf{f}_{\text{nonadia}}^\perp$ perpendicular to \mathbf{P} , i.e.,

$$\mathbf{f}_{\text{nonadia}}^\perp = \mathbf{f}_{\text{nonadia}} - \frac{\mathbf{f}_{\text{nonadia}} \cdot \mathbf{P}}{\mathbf{P} \cdot \mathbf{P}} \mathbf{P}. \quad (\text{S13})$$

Numerical Integrator for SQC-TW and Ehrenfest Dynamics

In contrast to the aforementioned NaF integrator, SQC-TW and Ehrenfest dynamics employ the mean force picture rather than the nonadiabatic force picture. In this picture, the integrator includes Steps 1, 2, 3, and 5 of the NaF/NaF-TW integrator. Unlike NaF/NaF-TW, for SQC-TW and Ehrenfest dynamics, the full nuclear force (i.e., the time derivative of \mathbf{P}) in Steps 1 and 5 is defined as

$$\dot{\mathbf{P}} = \mathbf{f}_{\text{mf}}(t) = -\sum_{k,l} \left[\nabla_{\mathbf{R}} E_k(\mathbf{R}_t) \delta_{kl} + (E_k(\mathbf{R}_t) - E_l(\mathbf{R}_t)) \mathbf{d}_{lk}(\mathbf{R}_t) \right] \tilde{\rho}_{kl}(t). \quad (\text{S14})$$

For SQC-TW, $\tilde{\rho}(t) = \frac{1}{2} \tilde{\mathbf{g}}(t) \tilde{\mathbf{g}}^\dagger(t) - \tilde{\Gamma}(0)$, where the commutator matrix $\tilde{\Gamma}$ does *not* evolve with time. This is corresponding to the ‘zero-point energy adjustment’ treatment of the SQC-TW approach of Cotton and Miller in ref². (It should be noted that only the population-population correlation functions are corresponding to ref², and we propose the formulations of other kinds of time correlation functions; see the main text.) For Ehrenfest dynamics, $\tilde{\rho}(t) = \frac{1}{2} \tilde{\mathbf{g}}(t) \tilde{\mathbf{g}}^\dagger(t)$ is used.

Numerical Integrator for FSSH Dynamics

FSSH dynamics employs the adiabatic force picture rather than the nonadiabatic force picture, where the full nuclear force in Step 1 and Step 5 (of the numeric integrator of NaF/NaF-TW) is $\dot{\mathbf{P}} = \mathbf{f}_{\text{adia}}(t) = -\nabla_{\mathbf{R}} E_{j_{\text{occ}}(t)}(\mathbf{R}_t)$ instead. While in this approach, Step 4 (of the numeric integrator of NaF/NaF-TW) is replaced with the famous Fewest-Switches-Surface-Hopping algorithm^{3,4} (i.e., the eq (S51) of the Supporting Information of ref⁵) to determine a new occupied state $j_{\text{occ}}(t + \Delta t)$. The detailed description of the numerical integrator for FSSH dynamics can be found in Section S7 of the Supporting Information of ref⁶.

S2: Model Details

S2-A: Reduced Dynamics for System-Bath Models.

For system-bath models, the system is always bilinearly coupled with harmonic bath DOFs of a dissipative environment in the condensed phase. The system-bath coupling, representing the substantial influence from the bath environment, governs the dynamics of the system across a spectrum ranging from coherent to dissipative regimes. These models serve as pivotal tools for

understanding the electron/exciton dynamics in chemical and biological reactions. Numerically exact results of the spin-boson model can be achieved by quasi-adiabatic propagator path integral (QuAPI)⁷⁻⁹ and more efficient small matrix PI (SMatPI)^{10, 11}, hierarchy equations of motion (HEOM)¹²⁻¹⁶, (multi-layer) multi-configuration time-dependent Hartree [(ML-)MCTDH]¹⁷⁻¹⁹, and time-dependent density matrix renormalization group (TD-DMRG)²⁰.

Within this study, we test two distinctive models: the two-site spin-boson models and the seven-site Fenna–Matthews–Olson (FMO) Monomer model:

Spin-Boson Model: The two-site spin-boson models stand as a fundamental prototype for comprehension of electron transfer and energy transport phenomena. The Hamiltonian for spin-boson models reads $\hat{H} = \hat{H}_B + \hat{H}_{SB} + \hat{H}_S$ with employing the environment bath part \hat{H}_B , the linear coupling term \hat{H}_{S-B} and the system part \hat{H}_S as

$$\begin{aligned}\hat{H}_B &= \sum_{j=1}^{N_b} \frac{1}{2} (\hat{P}_j^2 + \omega_j^2 \hat{R}_j^2) \\ \hat{H}_{SB} &= \sum_{j=1}^{N_b} c_j \hat{R}_j (|1\rangle\langle 1| - |2\rangle\langle 2|) \\ \hat{H}_S &= \varepsilon (|1\rangle\langle 1| - |2\rangle\langle 2|) + \Delta (|1\rangle\langle 2| + |2\rangle\langle 1|)\end{aligned}\tag{S15}$$

Here ε denotes the energy bias while Δ signifies the tunneling between states $|1\rangle$ and $|2\rangle$. The bath is discretized into a series of quantum harmonic oscillators, with $\{\hat{P}_j\}$, $\{\hat{R}_j\}$, $\{\omega_j\}$ and $\{c_j\}$ representing the mass-weighted momentum, coordinate, frequencies and the coupling coefficients of the j -th oscillator, respectively. For spin-boson models, we adopt the discretization scheme proposed in refs^{21, 22} for the Ohmic spectral density $J(\omega) = \frac{\pi}{2} \alpha \omega \exp(-\omega / \omega_c)$ with the Kondo parameter α and the cut-off frequency ω_c , as depicted below:

$$\begin{cases} \omega_j = -\omega_c \ln\left(1 - \frac{j}{1+N_b}\right) \\ c_j = \omega_j \sqrt{\frac{\alpha\omega_c}{N_b+1}} \end{cases}, j=1, \dots, N_b. \quad (\text{S16})$$

In our simulation, we investigate four specific spin-boson models outlined in ref²³. These models span a range of system-bath coupling strengths from weak to strong (small to large α), and the cut-off frequency ω_c from low to high. Additionally, all simulations are conducted at low temperatures ($\beta = 5$) and utilize three hundred discrete bath modes to characterize the Ohmic spectral density within the spin-boson models.

FMO Monomer Model: The FMO complex derived from green sulfur bacteria serves as a prototype system crucial for investigating photosynthetic organisms²⁴⁻³¹. Specifically referencing ref²⁸, the FMO monomer employs a site-exciton model, encompassing a seven-site structure coupled with a harmonic bath, whose three parts of Hamiltonian alternatively reads,

$$\begin{aligned} \hat{H}_B &= \sum_{n=1}^F \sum_{j=1}^{N_b} (\hat{P}_{nj}^2 + \omega_j^2 \hat{R}_{nj}^2) / 2 \\ \hat{H}_{SB} &= \sum_{n=1}^F \sum_{j=1}^{N_b} c_j \hat{R}_{nj} |n\rangle \langle n| \\ \hat{H}_S &= \sum_{n,m=1}^F H_{S,mm} |n\rangle \langle m| \end{aligned} \quad (\text{S17})$$

$$= \begin{pmatrix} 12410 & -87.7 & 5.5 & -5.9 & 6.7 & -13.7 & -9.9 \\ -87.7 & 12530 & 30.8 & 8.2 & 0.7 & 11.8 & 4.3 \\ 5.5 & 30.8 & 12210 & -53.5 & -2.2 & -9.6 & 6.0 \\ -5.9 & 8.2 & -53.5 & 12320 & -70.7 & -17.0 & -63.3 \\ 6.7 & 0.7 & -2.2 & -70.7 & 12480 & 81.1 & -1.3 \\ -13.7 & 11.8 & -9.6 & -17.0 & 81.1 & 12630 & 39.7 \\ -9.9 & 4.3 & 6.0 & -63.3 & -1.3 & 39.7 & 12440 \end{pmatrix} \text{cm}^{-1}$$

Here the variables $\{\hat{P}_{nj}, \hat{R}_{nj}\}$ denote the mass-weighted momentum and coordinate of the j -th quantum harmonic oscillator for the bath on n -th site, and the bath frequencies $\{\omega_j\}$ and system-bath coupling coefficients $\{c_j\}$ are determined by discretizing the spectral density. Specifically, we utilize the Debye spectral density $J(\omega) = 2\lambda\omega_c\omega/(\omega^2 + \omega_c^2)$ for each site, with parameters $\lambda = 35 \text{ cm}^{-1}$ for the bath reorganization energy and $\omega_c = 106.14 \text{ cm}^{-1}$ for the characteristic frequency. The discretization scheme employed here is based on refs^{18, 32, 33}:

$$\begin{aligned}\omega_j &= \omega_c \tan\left(\frac{\pi}{2} - \frac{\pi j}{2(N_b + 1)}\right), \quad j = 1, \dots, N_b \\ c_j &= \omega_j \sqrt{\frac{2\lambda}{N_b + 1}}, \quad j = 1, \dots, N_b\end{aligned}\tag{S18}$$

A challenging temperature $T = 77\text{K}$ is investigated as studied in our previous work³⁴. The first site of the system is initially occupied, and the bath DOFs are sampled from the Wigner distributions of the corresponding harmonic oscillators. In the FMO monomer model, one hundred discrete bath modes per site (totaling $N_b = 100$) are used to represent the continuous Debye spectral density.

We consider the decoupled initial condition for both spin-boson models and FMO monomer model, where the system is in the excited state and the bath modes are at the thermal equilibrium (i.e., the quantum Boltzmann distribution for the pure bath Hamiltonian operator). Specially, the bath modes are sampled from the corresponding Wigner distribution

$$\rho_W(\mathbf{R}, \mathbf{P}) \propto \exp\left[-\sum_{j=1}^{N_b} \frac{\beta}{2Q(\omega_j)} (P_j^2 + \omega_j^2 R_j^2)\right]\tag{S19}$$

with $Q(\omega) = \frac{\beta\hbar\omega/2}{\tanh(\beta\hbar\omega/2)}$ as the quantum corrector³⁵. For both the spin-boson models and the

FMO monomer model, we use the exact results obtained from our previous work²³ using HEOM/extended HEOM (eHEOM)^{36, 37} for comparison.

S2-B: Cavity Quantum Electrodynamics for Atom-in-Cavity Models.

It has been observed that several significant phenomena manifest in cavity quantum electrodynamics (cQED), particularly under conditions where matter is tightly coupled to the vacuum field within a confined optical cavity³⁸⁻⁴¹. In the main text, we examine benchmark cQED models featuring a multi-level hydrogen atom confined within a one-dimensional lossless cavity⁴²⁻⁴⁵. The atomic system is coupled to multi-cavity-modes, whose Hamiltonian is described by F atomic energy levels:

$$\hat{H} = \sum_{n=1}^F \varepsilon_n |n\rangle\langle n| + \sum_{j=1}^N \frac{1}{2} (\hat{P}_j^2 + \omega_j^2 \hat{R}_j^2) + \sum_{j=1}^N \omega_j \lambda_j(r_0) \hat{R}_j \sum_{n \neq m}^F \mu_{nm} |n\rangle\langle m|, \quad (\text{S20})$$

where ε_n is the atomic energy level of the n -th atomic state, and we employ a three-state model with the energy levels $\varepsilon_1 = -0.6738$, $\varepsilon_2 = -0.2798$, $\varepsilon_3 = -0.1547$, and μ_{nm} denotes the transitional dipole moment with nonzero values $\mu_{12} = -1.034$, $\mu_{23} = -2.536$ (all in atomic units).

The first model involves full three atomic levels, and the second one is a reduced two-level model where only the two lowest levels are considered. The variables $\hat{R}_j, \hat{P}_j, \omega_j$ denote the canonical coordinate, canonical momentum, and frequency of the j -th optical field mode, respectively, and the atom-optical field interaction reads

$$\lambda_j(r_0) = \sqrt{\frac{2}{\varepsilon_0 L}} \sin\left(\frac{j\pi r_0}{L}\right), \quad j = 1, \dots, N, \quad (\text{S21})$$

where L , ε_0 and r_0 denote the volume length of cavity, the vacuum permittivity, and the location of the atom, respectively. We fix $L = 236200$ a.u. and $r_0 = L/2$, and employ four hundred standing-wave modes for the optical field, with the frequency ω_j of the j -th mode set to $j\pi c/L$ (Here $c = 137.036$ a.u. denotes the light speed in vacuum). Initially, the highest atomic level is excited, while all cavity modes remain in the vacuum state. Subsequently, spontaneous emission occurs, releasing a photon that traverses the cavity and reflects back to interact with the atom. This sequence is followed by re-absorption and re-emission process. We compare our results with benchmark data obtained from truncated configuration interaction calculations, as reported in refs 42, 43.

S2-C: Dynamics around Conical Intersection for Linear Vibronic Coupling Models.

The linear vibronic coupling model (LVCM) is a straightforward yet powerful model that simulates molecular systems, particularly those where the conical intersection (CI) region is pivotal, such as in light-induced processes. In the diabatic representation, the Hamiltonian of LVCM is expressed as

$$\hat{H} = \sum_{k=1}^N \frac{\omega_k}{2} (\hat{P}_k^2 + \hat{R}_k^2) + \sum_{n=1}^F \left(E_n + \sum_{k=1}^N \kappa_k^{(n)} \hat{R}_k \right) |n\rangle\langle n| + \sum_{n \neq m}^F \left(\sum_{k=1}^N \lambda_k^{(nm)} \hat{R}_k \right) |n\rangle\langle m|, \quad (\text{S22})$$

where E_n ($n=1, \dots, F$) is the vertical excitation energy of the n -th state, while \hat{P}_k and \hat{R}_k ($k=1, \dots, N$) denote dimensionless weighted normal-mode momentum and coordinate of the k -th nuclear DOF, respectively, with the corresponding frequency ω_k . Additionally, the parameters $\kappa_k^{(n)}$ and $\lambda_k^{(nm)}$ represent the linear coupling coefficients of the k -th nuclear vibronic DOF with the diagonal and off-diagonal elements of the electronic density, respectively.

In our first case study, we explore two versions of the linear vibronic coupling model (LVCM) applied to the S1/S2 conical intersection of the pyrazine molecule. One LVCM variant includes three nuclear modes, while the other incorporates 24 nuclear modes. Detailed parameters for these models can be found in refs ^{46,47}. The initial state consists of the cross-product between the vibronic ground state and the electronically excited diabatic state (S2). Furthermore, we investigate a typical three-electronic-state LVCM with two nuclear modes for the Cr(CO)₅ molecule, as detailed in ref ⁴⁸. Here, the initial condition comprises the cross-product of the first electronically excited diabatic state and a Gaussian nuclear wave-packet. The Gaussian wave-packet is centered at the minimum point of the ground state of the Cr(CO)₆ molecule, where a carbonyl group dissociates. The width of each mode is determined by the corresponding vibrational frequencies. While we employ the diabatic representation for initializing and evaluating dynamical properties, consistent with the approach in MCTDH, we switch to the adiabatic representation for real-time dynamics to ensure fair comparison among different non-adiabatic dynamics methods. The parameter lists for the LVCMs applied to both the pyrazine and Cr(CO)₅ molecules can be found in the Supporting Information, specifically in Tables S2-S4 of ref ⁴⁹.

S2-D: Photodissociation Dynamics of Gas Phase Models with One Nuclear Degree of Freedom.

We further test NaF and NaF-TW for gas phase models with asymptotic regions. We consider the coupled three-electronic-state photodissociation models of Miller and coworkers ⁵⁰. Each PES is described by a Morse oscillator and the coupling terms are depicted by Gaussian functions:

$$\begin{aligned}
 V_{ii}(R) &= D_i \left[1 - e^{-\beta_i(R-R_i)} \right]^2 + C_i, \quad i = 1, 2, 3, \\
 V_{ij}(R) &= V_{ji}(R) = A_{ij} e^{-\alpha_{ij}(R-R_{ij})^2}, \quad i, j = 1, 2, 3; \text{ and } i \neq j.
 \end{aligned}
 \tag{S23}$$

where the detailed parameters match those of Model III as described in ref ⁵⁰. The Wigner distribution for nuclear DOF is $\rho_W(R, P) \propto e^{-m\omega(R-R_e)^2 - P^2/m\omega}$, where $m = 20000$ a.u. is the mass of the nuclear DOF, $\omega = 0.005$ a.u. is the vibrational frequency of ground state, and R_e denotes the center of wavepacket. The initial occupation is in the first electronic diabatic state. Numerically exact results for the models can be obtained by the discrete variable representation (DVR) approach⁵¹.

S2-E: Nonadiabatic Scattering Dynamics of Tully’s Models.

We investigate the performance of trajectory dynamics for Tully’s three models⁴ for nonadiabatic scattering dynamics, namely, the single avoided crossing (SAC) model, the dual avoided crossing (DAC) model and the extended coupling region (ECR) model. The results of the ECR model are demonstrated in the main text. The ECR model poses a formidable challenge for mapping-based methods, involving some trajectories that transmit forward while others reflect—a complex scenario inadequately described within mean-field approximations. The Hamiltonian of ECR model reads

$$\begin{aligned} V_{11}(R) &= +E_0 \\ V_{22}(R) &= -E_0 \\ V_{12}(R) &= V_{21}(R) = C[e^{BR}h(-R) + (2 - e^{-BR})h(R)] \end{aligned}, \quad (\text{S24})$$

where $B = 0.9$, $C = 0.1$, $E_0 = -0.0006$, and $h(R)$ represents the Heaviside function. Initially, the system with mass $m = 2000$ a.u. occupies in the electronic adiabatic ground state, and the nuclear wavefunction $\psi(R) \propto e^{-\alpha(R-R_0)^2/2 + iP_0(R-R_0)}$ leads to the corresponding Wigner distribution $\rho_W(R, P) \propto e^{-\alpha(R-R_0)^2 + (P-P_0)^2/\alpha}$. The center of the wavefunction, denoted by R_0 , is positioned at -13 , with a width parameter of $\alpha = 1$. The initial momentum is set to P_0 varying from 2 to 50.

In addition, we also provide supplemental results of trajectory-based dynamics for the SAC model and the DAC model⁴. The SAC model reads

$$\begin{aligned}
 V_{11}(R) &= A(1 - e^{-B|R|}) \operatorname{sgn}(R) \\
 V_{22}(R) &= -V_{11}(R) \\
 V_{12}(R) &= V_{21}(R) = Ce^{-DR^2}
 \end{aligned} \tag{S25}$$

with $A = 0.01$, $B = 1.6$, $C = 0.005$, $D = 1.0$, and initial $R_0 = -3.8$; and the DAC model reads

$$\begin{aligned}
 V_{11}(R) &= 0 \\
 V_{22}(R) &= -Ae^{-BR^2} + E_0 \\
 V_{12}(R) &= V_{21}(R) = Ce^{-DR^2}
 \end{aligned} \tag{S26}$$

with $A = 0.1$, $B = 0.28$, $C = 0.015$, $D = 0.06$, $E_0 = 0.05$ and initial $R_0 = -10$. Other parameters keep the same as those used in the ECR model. Figure S1 presents the transmission probabilities of the SAC and the DAC models. For the SAC model, the results of all methods are close to each other. For the DAC model, the phase space dynamics (NaF, SQC-TW and NaF-TW) slightly outperform Ehrenfest dynamics and FSSH dynamics, especially in the high kinematic energy region where $P_0 > 20$.

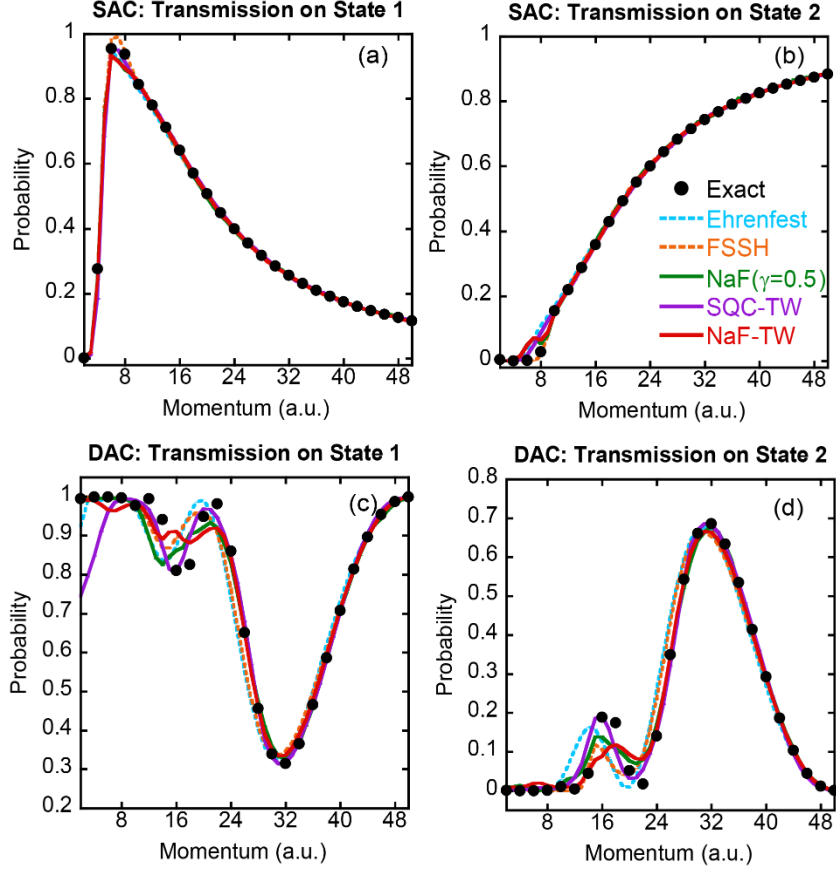


Figure S1. Panels (a-b) describe the transmission probability on (adiabatic) State 1 and that on State 2 for Tully’s SAC model. Panels (c-d) present the transmission probability on (adiabatic) State 1 and that on State 2 for Tully’s DAC model. Black points: Exact results produced by DVR. Cyan long-dashed lines: Ehrenfest dynamics. Orange short-dashed lines: FSSH. Green, purple, and red solid lines respectively illustrate NaF, SQC-TW, and NaF-TW dynamics.

S2-F: Electron Transfer Rate in Condensed Phase

We apply NaF-TW to calculate the electron transfer rate in condensed phase. We adopt the model employed in refs^{52,53}, which elucidates a two-level system coupled with a solvent bath:

$$\hat{H} = \hat{H}_s(\hat{R}_s, \hat{P}_s) + \hat{H}_b(\hat{\mathbf{R}}, \hat{\mathbf{P}}, \hat{R}_s, \hat{P}_s). \quad (\text{S27})$$

Here,

$$\begin{aligned} \hat{H}_s(\hat{R}_s, \hat{P}_s) = & \frac{1}{2}\hat{P}_s^2 + \left(\frac{1}{2}\varepsilon + \frac{1}{2}\Omega^2\hat{R}_s^2 + c_s\hat{R}_s\right)|1\rangle\langle 1| \\ & + \left(-\frac{1}{2}\varepsilon + \frac{1}{2}\Omega^2\hat{R}_s^2 - c_s\hat{R}_s\right)|2\rangle\langle 2| \quad , \\ & + \Delta(|1\rangle\langle 2| + |2\rangle\langle 1|) \end{aligned} \quad (\text{S28})$$

$$\hat{H}_b(\hat{\mathbf{R}}, \hat{\mathbf{P}}, \hat{R}_s, \hat{P}_s) = \sum_{n=1}^{N_b} \left[\frac{1}{2}\hat{P}_n^2 + \frac{1}{2}\omega_n^2 \left(\hat{R}_n + \frac{c_n}{\omega_n^2}\hat{R}_s \right)^2 \right], \quad (\text{S29})$$

where $\{\hat{P}_s, \hat{R}_s\}$ denote the nuclear momentum and coordinate of the reaction DOF, respectively, and $\{\hat{P}_n, \hat{R}_n\}$ ($n=1, \dots, N_b$) represent those of solvent bath DOFs. The frequencies $\{\omega_n\}$ and the coefficients $\{c_n\}$ ($n=1, \dots, N_b$) for solvent bath are obtained by discretizing the Ohmic spectral density with the Kondo parameter $\alpha = 9.49 \times 10^{-6}$ and the cut-off frequency $\omega_c = \Omega = 3.5 \times 10^{-4}$ a.u. The reorganization energy $\lambda = 2.39 \times 10^{-2}$ a.u., the coupling $\Delta = 5 \times 10^{-5}$ a.u., and the parameter $c_s = \Omega\sqrt{\lambda/2}$. One hundred discrete bath DOFs are utilized in the calculations.

The electron transfer rate is obtained from⁵⁴

$$k = \int_0^\infty dt \operatorname{Re} C_{FF}(t), \quad (\text{S30})$$

where the flux-flux correlation function is given by

$$C_{FF}(t) = \operatorname{Tr} \left[\hat{\rho}_n \hat{F} e^{i\hat{H}t} \hat{F} e^{-i\hat{H}t} \right], \quad (\text{S31})$$

with the flux operator defined as $\hat{F} = i\Delta(|1\rangle\langle 2| - |2\rangle\langle 1|)$. The initial density $\hat{\rho}_n$ for nuclear DOFs reads

$$\hat{\rho}_n \propto \exp\left[-\beta \sum_{n=1}^{N_b} (\hat{P}_n^2 + \omega_n^2 \hat{R}_n^2) / 2\right] \exp\left[-\beta (\hat{P}_s^2 / 2 + \Omega^2 \hat{R}_s^2 / 2 + c_s \hat{R}_s)\right], \quad (\text{S32})$$

with the temperature set at 300 K.

Given the scenario of weak coupling and relative high temperature, the Marcus electron transfer theory⁵⁵ is anticipated to perform reasonably well and is utilized as a benchmark. We also present the results from ref⁵³ obtained using an earlier version of SQC. Figure S2 depicts the relationship between the electronic transfer rate k and the bias ε . The results obtained from NaF-TW exhibit strong agreement with Marcus theory in both the normal and inverted regimes, and they show slightly better agreement compared to those of SQC in ref⁵³.

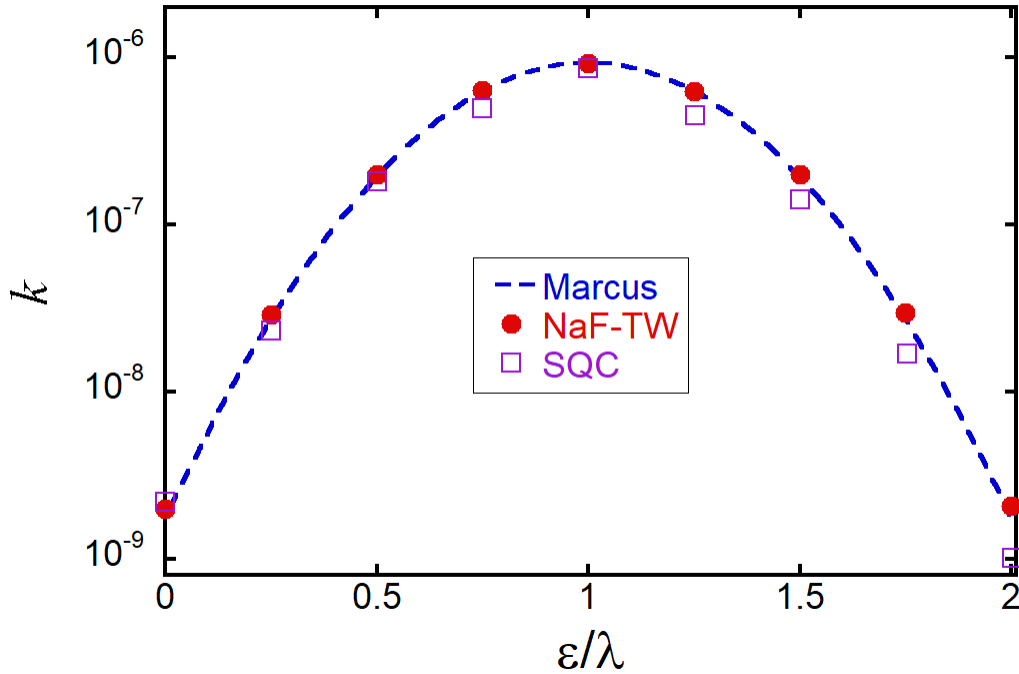


Figure S2. The electronic transfer rate k against ε/λ . Blue dashed line: Marcus theory. Red points: NaF-TW. Purple hollow squares: SQC taken from ref⁵³.

S3: Comparison of Different NaF-TW Strategies

In this section, we compare two NaF-TW strategies. The first, as presented in the main text, employs the scalar scheme for the initial condition of the commutator matrix, with the quasi-density matrix used as $\tilde{\rho} = (1 + F/3)\tilde{\mathbf{g}}\tilde{\mathbf{g}}^\dagger / \text{Tr}_e[\tilde{\mathbf{g}}\tilde{\mathbf{g}}^\dagger] - \mathbf{1}/3$. In the second approach, denoted as NaF-TW2, we may alternatively employ the full commutator matrix scheme, with the quasi-density matrix used as $\tilde{\rho} = \frac{1}{2}\tilde{\mathbf{g}}\tilde{\mathbf{g}}^\dagger - \tilde{\Gamma}$. NaF-TW and NaF-TW2 schemes exhibit nearly comparable performance across all benchmark models. In Figure S3 and S4, we compare their performance using the spin-boson model and LVCM model of pyrazine, respectively.

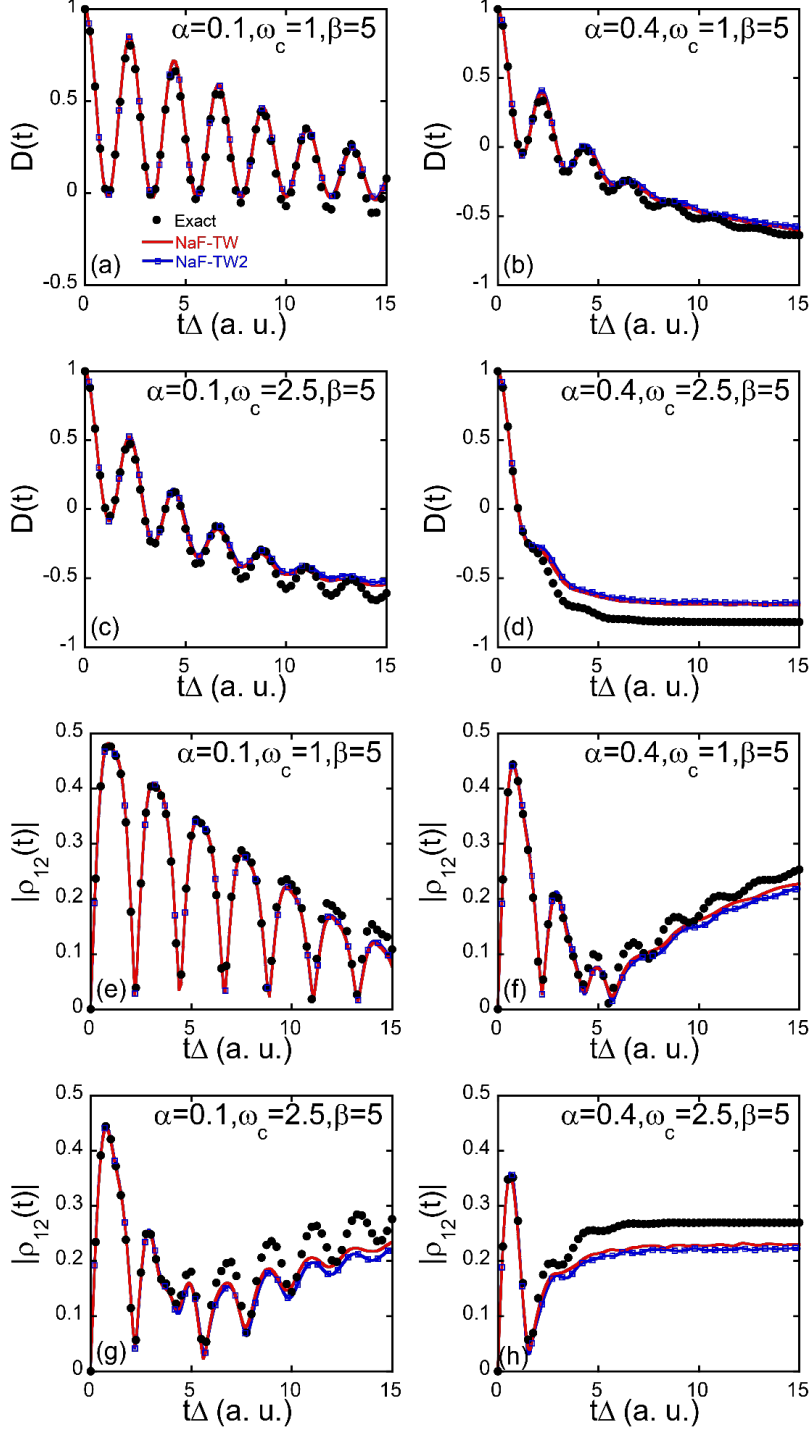


Figure S3. Comparison of the population dynamics (panels (a-d)) and coherence dynamics (panels (e-h)) of NaF-TW and NaF-TW2 for four spin-boson models discussed in the main text. The parameters for the models in panels (a-h) are consistent with those detailed in Figure 1 of the main

text. Red lines indicate: NaF-TW. Blue lines with hollow squares: NaF-TW2. Exact numerical results are denoted by black points.

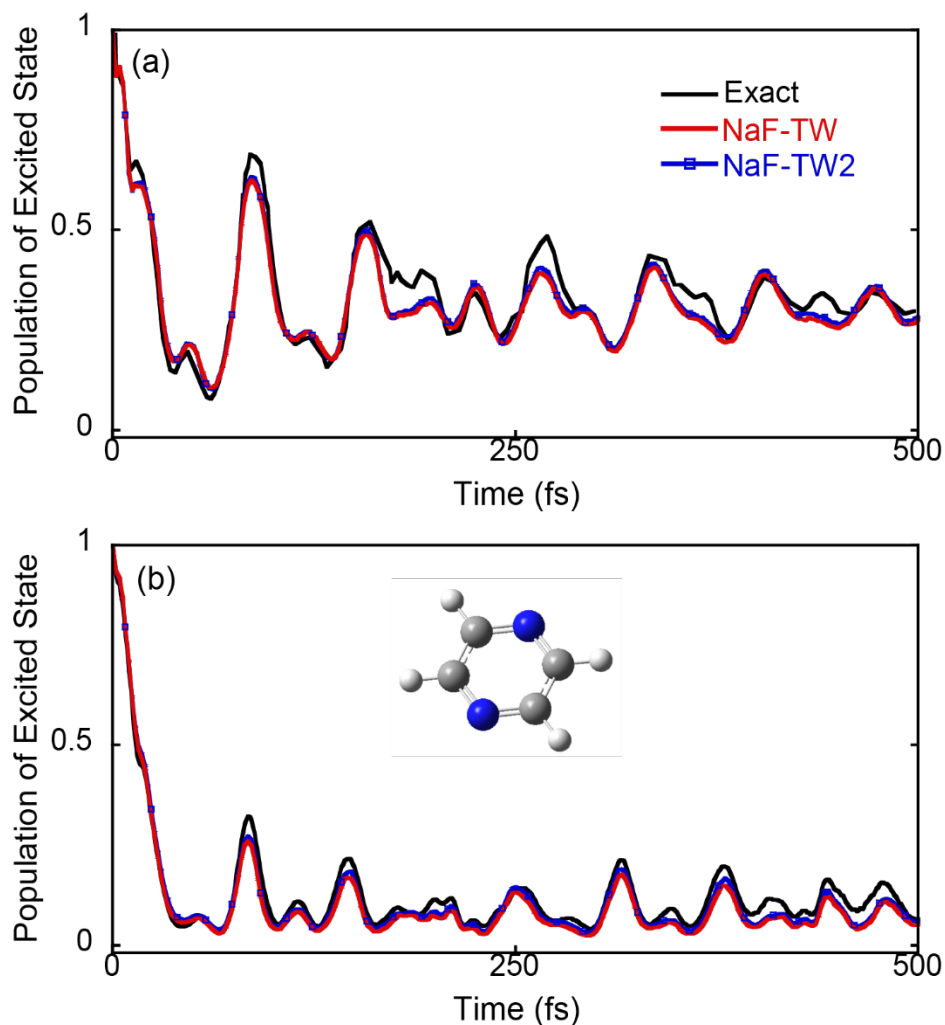


Figure S4. Comparisons of NaF-TW and NaF-TW2. Panels (a-b) depict the population dynamics of the second state of the 2-state LVCM with 3 modes for pyrazine⁴⁶ and that with 24 modes for the same molecule⁴⁷, respectively. Red lines: NaF-TW. Blue lines with hollow squares: NaF-TW2. Black lines: Exact numerical results produced by MCTDH⁵⁶.

S4: Proof of Exact Time Correlation Functions Involving Coherence Terms for Pure Multi-Electronic-State Systems

In the main text, we have proposed a set of expressions of time correlation functions involving coherence terms, as shown in eqs (10), (12), (14)-(15) and (18)-(21). For pure multi-electronic-state systems, one can utilize the transformation eq (S1) to obtain the expression of population-coherence correlation functions: for $k \neq l$,

$$\begin{aligned}
& \text{Tr}_e \left[|n\rangle \langle n| e^{i\hat{H}t} |k\rangle \langle l| e^{-i\hat{H}t} \right] \\
& \mapsto \int \frac{2d\mathbf{x}_0 d\mathbf{p}_0}{(2\pi)^F \left(2 - \frac{1}{2} \left((x_0^{(n)})^2 + (p_0^{(n)})^2 \right) \right)^{F-2}} K_{nn}^{\text{SQC}}(\mathbf{x}_0, \mathbf{p}_0) K_{lk}^{\text{CMM}}(\mathbf{x}_t, \mathbf{p}_t), \quad (\text{S33}) \\
& = \int \frac{2d\mathbf{e}_0 d\boldsymbol{\theta}_0}{(2\pi)^F \left(2 - e_0^{(n)} \right)^{F-2}} K_{nn}^{\text{SQC}}(\mathbf{e}_0, \boldsymbol{\theta}_0) K_{lk}^{\text{CMM}}(\mathbf{e}_t, \boldsymbol{\theta}_t)
\end{aligned}$$

where

$$K_{nn}^{\text{SQC}}(\mathbf{e}, \boldsymbol{\theta}) \equiv K_{nn}^{\text{SQC}}(\mathbf{e}) = h(e^{(k)} - 1) \prod_{k' \neq k} h(2 - e^{(k)} - e^{(k')}) \quad (\text{S34})$$

and

$$K_{lk}^{\text{CMM}}(\mathbf{e}, \boldsymbol{\theta}) = \sqrt{e^{(l)} e^{(k)}} e^{i(\theta^{(l)} - \theta^{(k)})} \quad (\text{S35})$$

are derived from substituting eq (S1) into eqs (14)-(15) and eq (19) of the main text.

For $n \neq m$, the coherence-population and coherence-coherence correlation functions read

$$\begin{aligned}
& \text{Tr}_e \left[|n\rangle \langle m| e^{i\hat{H}t} |k\rangle \langle l| e^{-i\hat{H}t} \right] \\
& \mapsto \int \frac{12d\mathbf{x}_0 d\mathbf{p}_0}{5(2\pi)^F} \sum_{i=n,m} \frac{K_{ii}^{\text{SQC}}(\mathbf{x}_0, \mathbf{p}_0)}{\left(2 - \frac{1}{2} \left((x_0^{(i)})^2 + (p_0^{(i)})^2 \right) \right)^{F-2}} K_{mn}^{\text{CMM}}(\mathbf{x}_0, \mathbf{p}_0) K_{lk}^{\text{CMM}}(\mathbf{x}_t, \mathbf{p}_t). \quad (\text{S36}) \\
& = \int \frac{12d\mathbf{e}_0 d\boldsymbol{\theta}_0}{5(2\pi)^F} \sum_{i=n,m} \frac{K_{ii}^{\text{SQC}}(\mathbf{e}_0, \boldsymbol{\theta}_0)}{\left(2 - e_0^{(i)} \right)^{F-2}} K_{mn}^{\text{CMM}}(\mathbf{e}_0, \boldsymbol{\theta}_0) K_{lk}^{\text{CMM}}(\mathbf{e}_t, \boldsymbol{\theta}_t)
\end{aligned}$$

The exact time correlation functions read

$$\text{Tr}_e \left[|n\rangle \langle m| e^{i\hat{H}t} |k\rangle \langle l| e^{-i\hat{H}t} \right] = \mathbf{U}(t)_{ln} \mathbf{U}(t)_{km}^*, \quad (\text{S37})$$

where the time evolution operator $e^{-i\hat{H}t}$ is represented by a unitary matrix $\mathbf{U}(t) = e^{-iVt}$. In this section, we prove that the correlation functions eqs (S33) and (S36) for pure electronic DOFs are exact, when the equations of motion of mapping variables read

$$\dot{\mathbf{g}} = -i\mathbf{V}\mathbf{g}, \quad (\text{S38})$$

whose solution reads

$$\mathbf{g}_t = \mathbf{U}(t)\mathbf{g}_0 \equiv e^{-iVt}\mathbf{g}_0. \quad (\text{S39})$$

Corresponding to eq (S39), the time evolution of off-diagonal (i.e., $l \neq k$) elements of CMM kernel reads

$$\begin{aligned} K_{lk}^{\text{CMM}}(\mathbf{e}_t, \boldsymbol{\theta}_t) &= K_{lk}^{\text{CMM}}(\mathbf{x}_t, \mathbf{p}_t) \\ &= \frac{1}{2}(x_t^{(l)} + ip_t^{(l)})(x_t^{(k)} - ip_t^{(k)}) \\ &= \frac{1}{2}(\mathbf{U}(t)\mathbf{g}_0)_l (\mathbf{g}_0^\dagger \mathbf{U}^\dagger(t))_k \\ &= \sum_{r,s=1}^F \mathbf{U}(t)_{lr} \mathbf{U}^*(t)_{ks} \sqrt{e_0^{(r)} e_0^{(s)}} e^{i(\theta_0^{(r)} - \theta_0^{(s)})} \end{aligned} \quad (\text{S40})$$

1) the exact *population-coherence* correlation functions for pure electronic dynamics:

When only electronic DOFs are involved, using eq (S40), and also utilizing that for any $\theta_0^{(k)}, k = 1, \dots, F$, and integer m ,

$$\int_0^{2\pi} e^{im\theta_0^{(k)}} d\theta_0^{(k)} = 2\pi\delta_{m0} = \delta_{m0} \int_0^{2\pi} d\theta_0^{(k)}, \quad (\text{S41})$$

the population-coherence correlation functions eq (S33) undergo the following transformation,

$$\begin{aligned}
& \int \frac{2d\mathbf{e}_0 d\boldsymbol{\theta}_0}{(2\pi)^F (2 - e_0^{(n)})^{F-2}} K_{nn}^{\text{SQC}}(\mathbf{e}_0, \boldsymbol{\theta}_0) K_{lk}^{\text{CMM}}(\mathbf{e}_t, \boldsymbol{\theta}_t) \\
&= \int \frac{2d\mathbf{e}_0 d\boldsymbol{\theta}_0}{(2\pi)^F (2 - e_0^{(n)})^{F-2}} K_{nn}^{\text{SQC}}(\mathbf{e}_0) \sum_{r,s=1}^F \mathbf{U}(t)_{lr} \mathbf{U}^*(t)_{ks} \sqrt{e_0^{(r)} e_0^{(s)}} e^{i(\theta_0^{(r)} - \theta_0^{(s)})}. \quad (\text{S42}) \\
&= \int \frac{2d\mathbf{e}_0}{(2 - e_0^{(n)})^{F-2}} K_{nn}^{\text{SQC}}(\mathbf{e}_0) \sum_{r=1}^F \mathbf{U}(t)_{lr} \mathbf{U}^*(t)_{kr} e_0^{(r)}
\end{aligned}$$

Then, using the properties that for $l \neq k$, $\sum_{r=1}^F \mathbf{U}(t)_{lr} \mathbf{U}^*(t)_{kr} = 0$ and that for any $r \neq s \neq n$,

$$\int \frac{2d\mathbf{e}}{(2 - e^{(n)})^{F-2}} K_{nn}^{\text{SQC}}(\mathbf{e}) e^{(r)} = \int \frac{2d\mathbf{e}}{(2 - e^{(n)})^{F-2}} K_{nn}^{\text{SQC}}(\mathbf{e}) e^{(s)}. \quad (\text{S43})$$

equation (S42) is transformed to

$$\begin{aligned}
& \int \frac{2d\mathbf{e}_0}{(2 - e_0^{(n)})^{F-2}} K_{nn}^{\text{SQC}}(\mathbf{e}_0) \sum_{r=1}^F \mathbf{U}(t)_{lr} \mathbf{U}^*(t)_{kr} e_0^{(r)} \\
&= \mathbf{U}(t)_{ln} \mathbf{U}^*(t)_{kn} \int \frac{2d\mathbf{e}_0}{(2 - e_0^{(n)})^{F-2}} K_{nn}^{\text{SQC}}(\mathbf{e}_0) (e_0^{(n)} - e_0^{(r \neq n)})
\end{aligned} \quad (\text{S44})$$

Cotton and Miller had obtained the following integrals in ref¹,

$$\begin{aligned}
& \int \frac{2d\mathbf{e}}{(2 - e^{(n)})^{F-2}} K_{nn}^{\text{SQC}}(\mathbf{e}) e^{(n)} \\
&= \int_1^2 2d\mathbf{e}^{(n)} e^{(n)} (2 - e^{(n)})^{2-F} \prod_{n' \neq n} \int_0^{2 - e^{(n)}} d\mathbf{e}^{(n')}, \quad (\text{S45}) \\
&= \frac{4}{3}
\end{aligned}$$

and

$$\begin{aligned}
& \int \frac{2d\mathbf{e}}{(2-e^{(n)})^{F-2}} K_{nn}^{\text{SQC}}(\mathbf{e}) e^{(r \neq n)} \\
&= \int_1^2 2de^{(n)} (2-e^{(n)})^{2-F} \int_0^{2-e^{(n)}} de^{(r)} e^{(r)} \prod_{n' \neq \{n, r\}} \int_0^{2-e^{(n)}} de^{(n')} . \\
&= \frac{1}{3}
\end{aligned} \tag{S46}$$

Substituting eqs (S45) and (S46) into eq (S44), we obtain

$$\begin{aligned}
& \int \frac{2d\mathbf{e}_0 d\boldsymbol{\theta}_0}{(2\pi)^F (2-e_0^{(n)})^{F-2}} K_{nn}^{\text{SQC}}(\mathbf{e}_0, \boldsymbol{\theta}_0) K_{lk}^{\text{CMM}}(\mathbf{e}_t, \boldsymbol{\theta}_t) \\
&= \mathbf{U}(t)_{ln} \mathbf{U}^*(t)_{kn} \left(\frac{4}{3} - \frac{1}{3} \right) \\
&= \text{Tr} \left[|n\rangle \langle n| e^{i\hat{H}t} |k\rangle \langle l| e^{-i\hat{H}t} \right]
\end{aligned} \tag{S47}$$

Thus, the population-coherence correlation functions are the same to the exact quantum results.

2) the exact *coherence-population* correlation functions and *coherence-coherence* correlation functions for pure electronic dynamics:

Utilizing eqs (S40)-(S41), for eq (S36) with $n \neq m$, we can also derive

$$\begin{aligned}
& \int \frac{12d\mathbf{e}_0 d\boldsymbol{\theta}_0}{5(2\pi)^F} \sum_{i=n, m} \frac{K_{ii}^{\text{SQC}}(\mathbf{e}_0, \boldsymbol{\theta}_0)}{(2-e_0^{(i)})^{F-2}} K_{mn}^{\text{CMM}}(\mathbf{e}_0, \boldsymbol{\theta}_0) K_{lk}^{\text{CMM}}(\mathbf{e}_t, \boldsymbol{\theta}_t) \\
&= \int \frac{12d\mathbf{e}_0 d\boldsymbol{\theta}_0}{5(2\pi)^F} \sum_{i=n, m} \frac{K_{ii}^{\text{SQC}}(\mathbf{e}_0, \boldsymbol{\theta}_0)}{(2-e_0^{(i)})^{F-2}} \sqrt{e_0^{(m)} e_0^{(n)}} e^{i(\theta_0^{(m)} - \theta_0^{(n)})} \\
&\quad \times \sum_{r, s=1}^F \mathbf{U}(t)_{lr} \mathbf{U}^*(t)_{ks} \sqrt{e_0^{(r)} e_0^{(s)}} e^{i(\theta_0^{(r)} - \theta_0^{(s)})} \\
&= \mathbf{U}(t)_{ln} \mathbf{U}^*(t)_{km} \int \frac{12d\mathbf{e}_0}{5} \sum_{i=n, m} \frac{K_{ii}^{\text{SQC}}(\mathbf{e}_0)}{(2-e_0^{(i)})^{F-2}} e_0^{(m)} e_0^{(n)}
\end{aligned} \tag{S48}$$

we can derive that

$$\begin{aligned}
& \int 2d\mathbf{e} \frac{K_{kk}^{\text{SQC}}(\mathbf{e})}{(2-e^{(k)})^{F-2}} e^{(k)} e^{(j \neq k)} \\
&= \int_1^2 2de^{(k)} e^{(k)} (2-e^{(k)})^{2-F} \int_0^{2-e^{(k)}} d\mathbf{e}^{(j)} e^{(j)} \prod_{k' \neq \{j, k\}} \int_0^{2-e^{(k)}} d\mathbf{e}^{(k')} . \\
&= \frac{5}{12}
\end{aligned} \tag{S49}$$

Substituting eq (S49) into eq (S48), we obtain

$$\begin{aligned}
& \int \frac{12d\mathbf{e}_0 d\boldsymbol{\theta}_0}{5(2\pi)^F} \sum_{i=n, m} \frac{K_{ii}^{\text{SQC}}(\mathbf{e}_0, \boldsymbol{\theta}_0)}{(2-e_0^{(i)})^{F-2}} K_{mn}^{\text{CMM}}(\mathbf{e}_0, \boldsymbol{\theta}_0) K_{lk}^{\text{CMM}}(\mathbf{e}_t, \boldsymbol{\theta}_t) \\
&= \mathbf{U}(t)_{ln} \mathbf{U}^*(t)_{km} \left(\frac{6}{5} \times 2 \times \frac{5}{12} \right) , \\
&= \text{Tr} \left[|n\rangle \langle m| e^{i\hat{H}t/\hbar} |k\rangle \langle l| e^{-i\hat{H}t/\hbar} \right]
\end{aligned} \tag{S50}$$

so that the coherence-population correlation functions and coherence-coherence correlation functions are also exact for pure electronic dynamics.

S5: Alternative Phase Space Formulations Derived from Triangle Window Functions

We can transform the integrations on the action space of SQC-TW approach to integrations on single CPS surfaces. Observing that one phase space point at any time t always lies on a particular

iso-action line $\sum_{n=1}^F e^{(n)} = \lambda$, the integral on the action space can be expressed as

$$\begin{aligned}
& \int_0^{+\infty} d\bar{e}^{(1)} \dots d\bar{e}^{(F)} f(\bar{e}^{(1)}, \dots, \bar{e}^{(F)}; \boldsymbol{\theta}) \\
&= \int_0^{+\infty} d\bar{\lambda} \int_0^{+\infty} d\bar{e}^{(1)} \dots d\bar{e}^{(F)} f(\bar{e}^{(1)}, \dots, \bar{e}^{(F)}; \boldsymbol{\theta}) \delta \left(\sum_{n=1}^F \bar{e}^{(n)} - \bar{\lambda} \right) \\
&\stackrel{\bar{\lambda}=(1+F\gamma)\lambda}{=} \int_0^{+\infty} d\lambda \int_0^{+\infty} d\bar{e}^{(1)} \dots d\bar{e}^{(F)} f(\lambda e^{(1)}, \dots, \lambda e^{(F)}; \boldsymbol{\theta}) \delta \left(\sum_{n=1}^F e^{(n)} - (1+F\gamma) \right)
\end{aligned} \tag{S51}$$

The transformation $\{\bar{e}_0^{(i)}\} \mapsto \{\lambda e_0^{(i)}\}$ leads to $\{\bar{e}_t^{(i)}\} \mapsto \{\lambda e_t^{(i)}\}$ at any time t . We can then explicitly rewrite the integrals involved in the population-population correlation functions of electronic DOFs of the triangle window framework of Cotton and Miller^{1,2,57},

$$\begin{aligned}
p_{n \rightarrow m}^{\text{SQC}}(t) &\equiv \int \frac{2d\mathbf{e}_0 d\boldsymbol{\theta}_0}{(2\pi)^F (2 - e_0^{(n)})^{F-2}} K_{mm}^{\text{SQC}}(\mathbf{e}_0) K_{mm}^{\text{bin}}(\mathbf{e}_t) \\
&= \frac{(1+F\gamma)}{(2\pi)^F} \int F d\mathbf{e}_0 d\boldsymbol{\theta}_0 \delta\left(\sum_{k=1}^F e_0^{(k)} - (1+F\gamma)\right) \times \\
&\quad \int_0^{+\infty} \frac{2\lambda^{F-1}}{F(2-\lambda e_0^{(n)})^{F-2}} d\lambda h\left(\lambda - (e_0^{(n)})^{-1}\right) h\left(2(e_0^{(n)})^{-1} - \lambda\right) \prod_{n' \neq n} h\left(\frac{2}{e_0^{(n')} + e_0^{(n)}} - \lambda\right), \quad (\text{S52}) \\
&\quad h\left(\lambda - (e_t^{(m)})^{-1}\right) \prod_{m' \neq m} h\left((e_t^{(m')})^{-1} - \lambda\right) \\
&= \frac{(1+F\gamma)}{(2\pi)^F} \int F d\mathbf{e}_0 d\boldsymbol{\theta}_0 \delta\left(\sum_{k=1}^F e_0^{(k)} - (1+F\gamma)\right) \left[\int_{h_1}^{h_2} \frac{2\lambda^{F-1}}{F(2-\lambda e_0^{(n)})^{F-2}} d\lambda \right]_+
\end{aligned}$$

where the time-dependent boundaries h_1 and h_2 rely on the indexes n and m ,

$$\begin{aligned}
h_1 &= \max\left\{(e_0^{(n)})^{-1}, (e_t^{(m)})^{-1}\right\}, \\
h_2 &= \min\left\{2(e_0^{(n)})^{-1}, \frac{2}{e_0^{(n')} + e_0^{(n)}}, (e_t^{(m')})^{-1} \mid n' \neq n, m' \neq m\right\}, \quad (\text{S53})
\end{aligned}$$

and $[a]_+ = \begin{cases} a, & \text{if } a > 0, \\ 0, & \text{otherwise} \end{cases}$. When $h_1 < h_2$ so that $p_{n \rightarrow m}^{\text{SQC}}(t) \neq 0$, $e_t^{(m)} > e_t^{(m')}$ for any $m' \neq m$. Also, at

time 0 the n -th state is occupied, thus $e_0^{(n)} > e_0^{(n')}$ for any $n' \neq n$. Noting that $\frac{2\lambda^{F-1}}{(2-\lambda e_0^{(n)})^{F-2}}$ is

monotonically increasing on the integrating domain of λ , we analytically evaluate that

$$\left[\int_{h_1}^{h_2} \frac{2\lambda^{F-1}}{F(2-\lambda e_0^{(n)})^{F-2}} d\lambda \right]_+ = \frac{(F-1)!}{F} \prod_{n' \neq n} h(e_0^{(n)} - e_0^{(n')}) \prod_{m' \neq m} h(e_t^{(m)} - e_t^{(m')}) \times \left[\phi \left(\min \left\{ \frac{2}{e_0^{(n')} + e_0^{(n)}}, \frac{1}{e_t^{(m')}} \mid n' \neq n, m' \neq m \right\}; e_0^{(n)} \right) - \phi \left(\max \left\{ \frac{1}{e_0^{(n)}}, \frac{1}{e_t^{(m)}} \right\}; e_0^{(n)} \right) \right]_+, \quad (\text{S54})$$

where

$$\phi(\lambda; e^{(n)}) = \lambda^F (2 - \lambda e^{(n)})^{1-F} \left(2(F-2)(F-1) {}_2\tilde{F}_1(1, 1; F+1; \lambda e^{(n)}/2) + \frac{(6-2F-\lambda e^{(n)})}{\Gamma(F)} \right). \quad (\text{S55})$$

Here, ${}_2\tilde{F}_1(a, b; c; z)$ is regularized hypergeometric function. Transforming back to the constraint phase space variables, the population-population correlation functions for electronic DOFs read

$$\text{Tr} \left[|n\rangle \langle n| e^{iHt} |m\rangle \langle m| e^{-iHt} \right] \mapsto \left(\bar{C}_{nm,mm}^{\text{sqz}}(t) \right)^{-1} \int_{\mathcal{S}} F d\mathbf{x}_0 d\mathbf{p}_0 \bar{W}_{nm,mm}^{\text{sqz}}(\mathbf{x}_0, \mathbf{p}_0; \mathbf{x}_t, \mathbf{p}_t) K_{nn}^{\text{sqz}}(\mathbf{x}_0, \mathbf{p}_0) K_{mm}^{\text{sqz}}(\mathbf{x}_t, \mathbf{p}_t) \quad (\text{S56})$$

where $K_{nn}^{\text{sqz}}(\mathbf{x}, \mathbf{p}) \equiv K_{nn}^{\text{sqz}}(\mathbf{e}, \boldsymbol{\theta}) = \prod_{n' \neq n} h(e^{(n)} - e^{(n')})$, the time-dependent normalization factor is

$$\bar{C}_{nm,mm}^{\text{sqz}}(t) = \sum_{k=1}^F \int_{\mathcal{S}} F d\mathbf{x}_0 d\mathbf{p}_0 \bar{W}_{nn,kk}^{\text{sqz}}(\mathbf{x}_0, \mathbf{p}_0; \mathbf{x}_t, \mathbf{p}_t) K_{nn}^{\text{sqz}}(\mathbf{x}_0, \mathbf{p}_0) K_{kk}^{\text{sqz}}(\mathbf{x}_t, \mathbf{p}_t) \quad (\text{S57})$$

and the generalized weight function is

$$\begin{aligned} \bar{W}_{nm,mm}^{\text{sqz}}(\mathbf{x}_0, \mathbf{p}_0; \mathbf{x}_t, \mathbf{p}_t) &\equiv \bar{W}_{nm,mm}^{\text{sqz}}(\mathbf{e}_0(\mathbf{x}_0, \mathbf{p}_0); \mathbf{e}_t(\mathbf{x}_t, \mathbf{p}_t)) \\ &= \frac{(1+F\gamma)^F}{F} \left[\phi \left(\min \left\{ \frac{2}{e_0^{(n' \neq n)} + e_0^{(n)}}, \frac{1}{e_t^{(m' \neq m)}} \mid n' \neq n, m' \neq m \right\}; e_0^{(n)} \right) - \phi \left(\max \left\{ \frac{1}{e_0^{(n)}}, \frac{1}{e_t^{(m)}} \right\}; e_0^{(n)} \right) \right]_+ \end{aligned} \quad (\text{S58})$$

for general F -state systems, which depends both on the values of $\mathbf{e}_0(\mathbf{x}_0, \mathbf{p}_0)$ and $\mathbf{e}_t(\mathbf{x}_t, \mathbf{p}_t)$.

Denoted as the Squeezed SQC (sqz) approach, within this formulation, the initial sampling is on the $U(F)/U(F-1)$ CPS denoted by $\mathcal{S}(\mathbf{x}, \mathbf{p}; \gamma)$, and the formulation involves a time-dependent denominator for population-population correlation terms.

Particularly, for the case $F = 2$, we derive $\phi(\lambda; e^{(n)}) = \lambda^2$, and correspondingly

$$\bar{w}_{m,mm}^{\text{sqz}}(\mathbf{x}_0, \mathbf{p}_0; \mathbf{x}_t, \mathbf{p}_t) \equiv \bar{w}_{mm,mm}^{\text{sqz}}(\mathbf{e}_0(\mathbf{x}_0, \mathbf{p}_0); \mathbf{e}_t(\mathbf{x}_t, \mathbf{p}_t)) = 2 - \frac{(1 + F\gamma)^2}{2 \min\{e_0^{(n)}, e_t^{(m)}\}^2}. \text{ This } F = 2 \text{ case of the}$$

formalism has been validated as a representation for *exact* population dynamics for pure two-state systems in ref⁵⁸.

■ AUTHOR INFORMATION

Corresponding Author

*E-mail: jianliupku@pku.edu.cn

ORCID

Xin He: 0000-0002-5189-7204

Xiangsong Cheng: 0000-0001-8793-5092

Baihua Wu: 0000-0002-1256-6859

Jian Liu: 0000-0002-2906-5858

Notes

The authors declare no competing financial interests.

■ ACKNOWLEDGMENT

This work was supported by the National Science Fund for Distinguished Young Scholars Grant No. 22225304. We acknowledge the High-performance Computing Platform of Peking University, Beijing PARATERA Tech Co., Ltd., and Guangzhou supercomputer center for providing computational resources. We thank Youhao Shang for useful discussions.

■ REFERENCES

- (1) Cotton, S. J.; Miller, W. H., A Symmetrical Quasi-Classical Windowing Model for the Molecular Dynamics Treatment of Non-Adiabatic Processes Involving Many Electronic States. *J. Chem. Phys.* **2019**, *150*, 104101. <http://dx.doi.org/10.1063/1.5087160>
- (2) Cotton, S. J.; Miller, W. H., Trajectory-Adjusted Electronic Zero Point Energy in Classical Meyer-Miller Vibronic Dynamics: Symmetrical Quasiclassical Application to Photodissociation. *J. Chem. Phys.* **2019**, *150*, 194110. <http://dx.doi.org/10.1063/1.5094458>
- (3) Tully, J. C.; Preston, R. K., Trajectory Surface Hopping Approach to Nonadiabatic Molecular Collisions: The Reaction of H⁺ with D₂. *J. Chem. Phys.* **1971**, *55*, 562-572. <http://dx.doi.org/10.1063/1.1675788>
- (4) Tully, J. C., Molecular Dynamics with Electronic Transitions. *J. Chem. Phys.* **1990**, *93*, 1061-1071. <http://dx.doi.org/10.1063/1.459170>
- (5) Wu, B.; He, X.; Liu, J., Nonadiabatic Field on Quantum Phase Space: A Century after Ehrenfest. *J. Phys. Chem. Lett.* **2024**, *15*, 644-658. <http://dx.doi.org/10.1021/acs.jpcllett.3c03385>
- (6) Wu, B.; He, X.; Liu, J., Phase Space Mapping Theory for Nonadiabatic Quantum Molecular Dynamics. In *Volume on Time-Dependent Density Functional Theory: Nonadiabatic Molecular Dynamics*, Zhu, C., Ed. Jenny Stanford Publishing: New York, 2022.
- (7) Makarov, D. E.; Makri, N., Path Integrals for Dissipative Systems by Tensor Multiplication. Condensed Phase Quantum Dynamics for Arbitrarily Long Time. *Chem. Phys. Lett.* **1994**, *221*, 482-491. [http://dx.doi.org/10.1016/0009-2614\(94\)00275-4](http://dx.doi.org/10.1016/0009-2614(94)00275-4)
- (8) Makri, N.; Makarov, D. E., Tensor Propagator for Iterative Quantum Time Evolution of Reduced Density Matrices. II. Numerical Methodology. *J. Chem. Phys.* **1995**, *102*, 4611-4618. <http://dx.doi.org/10.1063/1.469509>
- (9) Makri, N.; Makarov, D. E., Tensor Propagator for Iterative Quantum Time Evolution of Reduced Density Matrices. I. Theory. *J. Chem. Phys.* **1995**, *102*, 4600-4610. <http://dx.doi.org/10.1063/1.469508>
- (10) Makri, N., Small Matrix Path Integral with Extended Memory. *J. Chem. Theory. Comput.* **2021**, *17*, 1-6. <http://dx.doi.org/10.1021/acs.jctc.0c00987>
- (11) Makri, N., Small Matrix Disentanglement of the Path Integral: Overcoming the Exponential Tensor Scaling with Memory Length. *J. Chem. Phys.* **2020**, *152*, 041104. <http://dx.doi.org/10.1063/1.5139473>
- (12) Tanimura, Y.; Kubo, R., Time Evolution of a Quantum System in Contact with a Nearly Gaussian-Markoffian Noise Bath. *J. Phys. Soc. Jpn.* **1989**, *58*, 101-114. <http://dx.doi.org/10.1143/JPSJ.58.101>
- (13) Yan, Y.-A.; Yang, F.; Liu, Y.; Shao, J., Hierarchical Approach Based on Stochastic Decoupling to Dissipative Systems. *Chem. Phys. Lett.* **2004**, *395*, 216-221. <http://dx.doi.org/10.1016/j.cplett.2004.07.036>

- (14) Xu, R.-X.; Cui, P.; Li, X.-Q.; Mo, Y.; Yan, Y., Exact Quantum Master Equation Via the Calculus on Path Integrals. *J. Chem. Phys.* **2005**, *122*, 041103. <http://dx.doi.org/10.1063/1.1850899>
- (15) Shao, J., Stochastic Description of Quantum Open Systems: Formal Solution and Strong Dissipation Limit. *Chem. Phys.* **2006**, *322*, 187-192. <http://dx.doi.org/10.1016/j.chemphys.2005.08.007>
- (16) Moix, J. M.; Cao, J., A Hybrid Stochastic Hierarchy Equations of Motion Approach to Treat the Low Temperature Dynamics of Non-Markovian Open Quantum Systems. *J. Chem. Phys.* **2013**, *139*, 134106. <http://dx.doi.org/10.1063/1.4822043>
- (17) Meyer, H.-D.; Manthe, U.; Cederbaum, L. S., The Multi-Configurational Time-Dependent Hartree Approach. *Chem. Phys. Lett.* **1990**, *165*, 73-78. [http://dx.doi.org/10.1016/0009-2614\(90\)87014-i](http://dx.doi.org/10.1016/0009-2614(90)87014-i)
- (18) Thoss, M.; Wang, H.; Miller, W. H., Self-Consistent Hybrid Approach for Complex Systems: Application to the Spin-Boson Model with Debye Spectral Density. *J. Chem. Phys.* **2001**, *115*, 2991-3005. <http://dx.doi.org/10.1063/1.1385562>
- (19) Wang, H.; Thoss, M., Multilayer Formulation of the Multiconfiguration Time-Dependent Hartree Theory. *J. Chem. Phys.* **2003**, *119*, 1289-1299. <http://dx.doi.org/10.1063/1.1580111>
- (20) Ren, J. J.; Li, W. T.; Jiang, T.; Wang, Y. H.; Shuai, Z. G., Time-Dependent Density Matrix Renormalization Group Method for Quantum Dynamics in Complex Systems. *Wiley Interdiscip. Rev. Comput. Mol. Sci.* **2022**, *12*, e1614. <http://dx.doi.org/10.1002/wcms.1614>
- (21) Makri, N., The Linear Response Approximation and Its Lowest Order Corrections: An Influence Functional Approach. *J. Phys. Chem. B* **1999**, *103*, 2823-2829. <http://dx.doi.org/10.1021/jp9847540>
- (22) Wang, H., Iterative Calculation of Energy Eigenstates Employing the Multilayer Multiconfiguration Time-Dependent Hartree Theory. *J. Phys. Chem. A* **2014**, *118*, 9253-9261. <http://dx.doi.org/10.1021/jp503351t>
- (23) He, X.; Gong, Z.; Wu, B.; Liu, J., Negative Zero-Point-Energy Parameter in the Meyer-Miller Mapping Model for Nonadiabatic Dynamics. *J. Phys. Chem. Lett.* **2021**, *12*, 2496-2501. <http://dx.doi.org/10.1021/acs.jpcllett.1c00232>
- (24) Fenna, R. E.; Matthews, B. W., Chlorophyll Arrangement in a Bacteriochlorophyll Protein from Chlorobium-Limicola. *Nature* **1975**, *258*, 573-577. <http://dx.doi.org/10.1038/258573a0>
- (25) Engel, G. S.; Calhoun, T. R.; Read, E. L.; Ahn, T. K.; Mancal, T.; Cheng, Y. C.; Blankenship, R. E.; Fleming, G. R., Evidence for Wavelike Energy Transfer through Quantum Coherence in Photosynthetic Systems. *Nature* **2007**, *446*, 782-786. <http://dx.doi.org/10.1038/nature05678>
- (26) Maiuri, M.; Ostroumov, E. E.; Saer, R. G.; Blankenship, R. E.; Scholes, G. D., Coherent Wavepackets in the Fenna-Matthews-Olson Complex Are Robust to Excitonic-Structure

Perturbations Caused by Mutagenesis. *Nat. Chem.* **2018**, *10*, 177-183. <http://dx.doi.org/10.1038/Nchem.2910>

(27) Higgins, J. S.; Lloyd, L. T.; Sohail, S. H.; Allodi, M. A.; Otto, J. P.; Saer, R. G.; Wood, R. E.; Massey, S. C.; Ting, P. C.; Blankenship, R. E., et al., Photosynthesis Tunes Quantum-Mechanical Mixing of Electronic and Vibrational States to Steer Exciton Energy Transfer. *Proc. Natl. Acad. Sci.* **2021**, *118*, e2018240118. <http://dx.doi.org/10.1073/pnas.2018240118>

(28) Ishizaki, A.; Fleming, G. R., Theoretical Examination of Quantum Coherence in a Photosynthetic System at Physiological Temperature. *Proc. Natl. Acad. Sci.* **2009**, *106*, 17255-17260. <http://dx.doi.org/10.1073/pnas.0908989106>

(29) Tao, G.; Miller, W. H., Semiclassical Description of Electronic Excitation Population Transfer in a Model Photosynthetic System. *J. Phys. Chem. Lett.* **2010**, *1*, 891-894. <http://dx.doi.org/10.1021/jz1000825>

(30) Miller, W. H., Perspective: Quantum or Classical Coherence? *J. Chem. Phys.* **2012**, *136*, 210901. <http://dx.doi.org/10.1063/1.4727849>

(31) Cao, J. S.; Cogdell, R. J.; Coker, D. F.; Duan, H. G.; Hauer, J.; Kleinekathofer, U.; Jansen, T. L. C.; Mancal, T.; Miller, R. J. D.; Ogilvie, J. P., et al., Quantum Biology Revisited. *Sci. Adv.* **2020**, *6*, eaaz4888. <http://dx.doi.org/10.1126/sciadv.aaz4888>

(32) Wang, H.; Song, X.; Chandler, D.; Miller, W. H., Semiclassical Study of Electronically Nonadiabatic Dynamics in the Condensed-Phase: Spin-Boson Problem with Debye Spectral Density. *J. Chem. Phys.* **1999**, *110*, 4828-4840. <http://dx.doi.org/10.1063/1.478388>

(33) Craig, I. R.; Thoss, M.; Wang, H., Proton Transfer Reactions in Model Condensed-Phase Environments: Accurate Quantum Dynamics Using the Multilayer Multiconfiguration Time-Dependent Hartree Approach. *J. Chem. Phys.* **2007**, *127*, 144503. <http://dx.doi.org/10.1063/1.2772265>

(34) He, X.; Wu, B.; Gong, Z.; Liu, J., Commutator Matrix in Phase Space Mapping Models for Nonadiabatic Quantum Dynamics. *J. Phys. Chem. A* **2021**, *125*, 6845-6863. <http://dx.doi.org/10.1021/acs.jpca.1c04429>

(35) Liu, J.; Miller, W. H., A Simple Model for the Treatment of Imaginary Frequencies in Chemical Reaction Rates and Molecular Liquids. *J. Chem. Phys.* **2009**, *131*, 074113. <http://dx.doi.org/10.1063/1.3202438>

(36) Duan, C. R.; Tang, Z. F.; Cao, J. S.; Wu, J. L., Zero-Temperature Localization in a Sub-Ohmic Spin-Boson Model Investigated by an Extended Hierarchy Equation of Motion. *Phys. Rev. B* **2017**, *95*, 214308. <http://dx.doi.org/10.1103/PhysRevB.95.214308>

(37) Tang, Z.; Ouyang, X.; Gong, Z.; Wang, H.; Wu, J., Extended Hierarchy Equation of Motion for the Spin-Boson Model. *J. Chem. Phys.* **2015**, *143*, 224112. <http://dx.doi.org/10.1063/1.4936924>

- (38) Haugland, T. S.; Ronca, E.; Kjønsstad, E. F.; Rubio, A.; Koch, H., Coupled Cluster Theory for Molecular Polaritons: Changing Ground and Excited States. *Phys. Rev. X* **2020**, *10*, 041043. <http://dx.doi.org/10.1103/PhysRevX.10.041043>
- (39) Garcia-Vidal, F. J.; Ciuti, C.; Ebbesen, T. W., Manipulating Matter by Strong Coupling to Vacuum Fields. *Science* **2021**, *373*, eabd0336. <http://dx.doi.org/10.1126/science.abd0336>
- (40) Toida, H.; Nakajima, T.; Komiyama, S., Vacuum Rabi Splitting in a Semiconductor Circuit Qed System. *Phys. Rev. Lett.* **2013**, *110*, 066802. <http://dx.doi.org/10.1103/PhysRevLett.110.066802>
- (41) Guerin, W.; Santo, T.; Weiss, P.; Cipris, A.; Schachenmayer, J.; Kaiser, R.; Bachelard, R., Collective Multimode Vacuum Rabi Splitting. *Phys. Rev. Lett.* **2019**, *123*, 243401. <http://dx.doi.org/10.1103/PhysRevLett.123.243401>
- (42) Hoffmann, N. M.; Schafer, C.; Rubio, A.; Kelly, A.; Appel, H., Capturing Vacuum Fluctuations and Photon Correlations in Cavity Quantum Electrodynamics with Multitrajectory Ehrenfest Dynamics. *Phys. Rev. A* **2019**, *99*, 063819. <http://dx.doi.org/10.1103/PhysRevA.99.063819>
- (43) Hoffmann, N. M.; Schäfer, C.; Säkkinen, N.; Rubio, A.; Appel, H.; Kelly, A., Benchmarking Semiclassical and Perturbative Methods for Real-Time Simulations of Cavity-Bound Emission and Interference. *J. Chem. Phys.* **2019**, *151*, 244113. <http://dx.doi.org/10.1063/1.5128076>
- (44) Li, T. E.; Chen, H. T.; Nitzan, A.; Subotnik, J. E., Quasiclassical Modeling of Cavity Quantum Electrodynamics. *Phys. Rev. A* **2020**, *101*, 033831. <http://dx.doi.org/10.1103/PhysRevA.101.033831>
- (45) Saller, M. A. C.; Kelly, A.; Geva, E., Benchmarking Quasiclassical Mapping Hamiltonian Methods for Simulating Cavity-Modified Molecular Dynamics. *J. Phys. Chem. Lett.* **2021**, *12*, 3163-3170. <http://dx.doi.org/10.1021/acs.jpcclett.1c00158>
- (46) Schneider, R.; Domcke, W., S1-S2 Conical Intersection and Ultrafast S2->S1 Internal Conversion in Pyrazine. *Chem. Phys. Lett.* **1988**, *150*, 235-242. [http://dx.doi.org/10.1016/0009-2614\(88\)80034-4](http://dx.doi.org/10.1016/0009-2614(88)80034-4)
- (47) Kremppl, S.; Winterstetter, M.; Plöhn, H.; Domcke, W., Path-Integral Treatment of Multi-Mode Vibronic Coupling. *J. Chem. Phys.* **1994**, *100*, 926-937. <http://dx.doi.org/10.1063/1.467253>
- (48) Worth, G. A.; Welch, G.; Paterson, M. J., Wavepacket Dynamics Study of Cr(CO)₅ after Formation by Photodissociation: Relaxation through an (E ⊕ A) ⊗ e Jahn–Teller Conical Intersection. *Mol. Phys.* **2006**, *104*, 1095-1105. <http://dx.doi.org/10.1080/00268970500418182>
- (49) Wu, B.; He, X.; Liu, J., Nonadiabatic Field on Quantum Phase Space: A Century after Ehrenfest. *J. Phys. Chem. Lett.* **2024**, *15*, 644-658. <http://dx.doi.org/10.1021/acs.jpcclett.3c03385>
- (50) Coronado, E. A.; Xing, J.; Miller, W. H., Ultrafast Non-Adiabatic Dynamics of Systems with Multiple Surface Crossings: A Test of the Meyer-Miller Hamiltonian with Semiclassical

Initial Value Representation Methods. *Chem. Phys. Lett.* **2001**, *349*, 521-529. [http://dx.doi.org/10.1016/s0009-2614\(01\)01242-8](http://dx.doi.org/10.1016/s0009-2614(01)01242-8)

(51) Colbert, D. T.; Miller, W. H., A Novel Discrete Variable Representation for Quantum Mechanical Reactive Scattering Via the S-Matrix Kohn Method. *J. Chem. Phys.* **1992**, *96*, 1982-1991. <http://dx.doi.org/10.1063/1.462100>

(52) Huo, P.; Miller, T. F.; Coker, D. F., Communication: Predictive Partial Linearized Path Integral Simulation of Condensed Phase Electron Transfer Dynamics. *J. Chem. Phys.* **2013**, *139*, 151103. <http://dx.doi.org/10.1063/1.4826163>

(53) Cotton, S. J.; Igumenshchev, K.; Miller, W. H., Symmetrical Windowing for Quantum States in Quasi-Classical Trajectory Simulations: Application to Electron Transfer. *J. Chem. Phys.* **2014**, *141*, 084104. <http://dx.doi.org/10.1063/1.4893345>

(54) Miller, W. H.; Schwartz, S. D.; Tromp, J. W., Quantum-Mechanical Rate Constants for Bimolecular Reactions. *J. Chem. Phys.* **1983**, *79*, 4889-4898. <http://dx.doi.org/10.1063/1.445581>

(55) Marcus, R. A., On the Theory of Electron-Transfer Reactions. VI. Unified Treatment for Homogeneous and Electrode Reactions. *J. Chem. Phys.* **1965**, *43*, 679-701. <http://dx.doi.org/10.1063/1.1696792>

(56) Worth, G. A.; Beck, M. H.; Jackle, A.; Meyer, H.-D. The MCTDH Package, Version 8.2, (2000). H.-D. Meyer, Version 8.3 (2002), Version 8.4 (2007). O. Vendrell and H.-D. Meyer Version 8.5 (2013). Version 8.5 contains the ML-MCTDH algorithm. See <http://mctdh.uni-hd.de>. Used version: 8.5.14.

(57) Cotton, S. J.; Miller, W. H., A New Symmetrical Quasi-Classical Model for Electronically Non-Adiabatic Processes: Application to the Case of Weak Non-Adiabatic Coupling. *J. Chem. Phys.* **2016**, *145*, 144108. <http://dx.doi.org/10.1063/1.4963914>

(58) Cheng, X.; He, X.; Liu, J., A Novel Class of Phase Space Representations for Exact Population Dynamics of Two-State Quantum Systems and the Relation to Symmetrical Window Functions. *Chinese J. Chem. Phys.* **2024**. **submitted**.